RESOURCE ADEQUACY IN GRIDS WITH INTEGRATED RENEWABLE RESOURCES

BY

MARIOLA NDRIO

THESIS

Submitted in partial fulfillment of the requirements
for the degree of Master of Science in Electrical and Computer Engineering
in the Graduate College of the
University of Illinois at Urbana-Champaign, 2017

Urbana, Illinois

Adviser:

Professor George Gross

ABSTRACT

The growing world-wide concern over the climate change manifests itself in the growth of grid-integrated renewable resources (RRs) to cost-effectively reduce greenhouse gas emissions and alleviate each nation's dependence on fuel imports. However, as the penetrations of RRs deepen into the electric power grids around the world, their impacts on the grid's resource adequacy become issues of growing concern. The marked intermittent and rapidly time-varying nature of RRs cannot be appropriately represented in the widely used time-invariant resource adequacy evaluation approach. In this thesis, we describe the development of a simulation-based resource adequacy evaluation framework with the capability to represent the uncertain and time-varying nature of the system loads, supply/demand resources, including those of renewable technologies. For this framework, we deploy stochastic-process-based models to effectively represent all grid-integrated resources so as to capture the intermittent, time-varying and uncertain nature of RRs and their correlation with loads and other resources. We make use of past load history and RR output data to construct the sample paths ($s.p.$s) associated with the stochastic process representations. The incorporation of RRs is based on the *net load* concept, which is defined to be the net difference between the total system load and the total RR outputs. In other words, the *net load* is the load that must be met by the conventional generation resources. Clearly, the *net load*, just as the system load and RRs, is itself a random process ($r.p.$) with $s.p.$s constructed from the $s.p.$s of the RR outputs and the loads. As such, the *net load*, in effect, captures the intermittent and time-varying nature of RRs. The time-varying framework uses Monte Carlo simulation techniques to sample the $r.p.$s of the loads, conventional unit availabilities and the RR outputs. In every simulation run, the efficient sampling of the $r.p.$s is used to construct the realizations of the outputs of the resources and loads and to evaluate the widely used resource adequacy metrics — the

loss of load probability ($LOLP$), the loss of load hours ($LOLH$), the loss of load expectation ($LOLE$) and the expected unserved energy (EUE). The multiple Monte Carlo simulation runs provide the statistical basis for the values of these metrics. The framework provides the capability to define and evaluate additional resource adequacy metrics that are particularly appropriate for the study of the RR impacts on resource adequacy. We introduce new sensitivity indices to quantify the impacts of deepening RR penetrations on the various metrics of interest. The new indices effectively capture the marginal behavior of the adequacy metrics and provide valuable insights to grid operators and planners into how each group of RRs affects each metric for a particular system. We applied the framework to study various resource adequacy issues on a set of large-scale systems. We present representative results from our extensive application studies on a realistic large-scale system with integrated wind and solar RRs, total installed capacity $40,000$ MW and projected summer peak load $36,800$ MW. The results provide detailed quantification of the behavior of the resource adequacy metrics as the RR penetrations deepen. Specifically, the results demonstrate the improvement in the grid's resource adequacy — indicated by the declining values of the metrics — as the penetrations of wind and solar deepen. An important finding is that solar resources appear to have a significantly more pronounced impact on the metrics than wind resources. Such findings make sense because of the generally good and consistent tracking of the load by the solar generation during the summer months for the summer peaking study system. However, the behavior of all the resource adequacy metrics is characterized by significant diminution of marginal returns as the penetrations of solar and wind deepen. Moreover, the tracking ability of solar during the peak summer months is insufficient to replace additional retirements of conventional generation capacity beyond a system-dependent value. Indeed, the resource adequacy of the system begins to deteriorate, i.e., the values of the metrics increase as the conventional capacity retirement increases. Notwithstanding deepening RR penetrations for the system discussed, when the ratio of the total retired conventional capacity over the total integrated RR capacity exceeds the 0.25 value, the inability of the grid to meet the "1 day in 10 years" resource adequacy criterion becomes evident. Such limitations of RRs in their ability to substitute retired conventional capacity and to provide resource adequacy, impact the retirement schedule of fossil-fired generation

units. The sensitivity studies carried out provide additional insights into the development of appropriate retirement schedules. A significant aspect of the thesis is the broad range of applications of the proposed framework to study both the short- and longer-time periods for planning, operations and other purposes. Furthermore, the framework allows for the evaluation of resource adequacy metrics for data even with different time resolutions. The proposed framework, provides a useful assessment mechanism to prepare large-grid operators in the transition to the greener electricity future.

To my brother George, who always believed in me

ACKNOWLEDGMENTS

I would like to express my sincere gratitude to my advisor, Professor George Gross, for giving me the amazing opportunity to study at the University of Illinois at Urbana-Champaign and fulfill one of my biggest dreams. I also thank Prof. Gross for his patience, support and guidance throughout my time as a graduate student. His truly impressive depth and breadth of knowledge on a wide range of subjects not only improved my technical understanding as a student, but also shaped my personality. I am particularly grateful to my advisor for teaching me, among many things, perseverance and discipline, critical thinking, attention to detail, how to better articulate my thoughts and to understand the qualities of great art.

I would also like to thank my dear and close friends Siddhartha Nigam, Adriano Lima Abrantes, Ogun Yurdakul, Raj Padmanabhan and Dimitra Apostolopoulou for the stimulating discussions, the encouragement and advice throughout my studies. Completing this thesis would have been all the more difficult were it not for their continuous support and friendship. Finally, I would like to thank my family for doing everything possible to enable me to follow my dreams.

TABLE OF CONTENTS

CHAPTER 1

INTRODUCTION

In this chapter we set the stage for the work presented in this thesis. Our research interests lie in the development of a resource adequacy evaluation framework with the explicit incorporation of renewable resources (*RR*s). The proposed framework allows for the consistent evaluation of the industry-wide resource adequacy metrics and the investigation of the impacts of the deepening *RR* penetrations in bulk power system reliability. We start out by providing an overview of the basic concepts in power system reliability and continue with the discussion of the motivation for our work and the background behind our research to allow the reader to better understand the nature of the problem considered. We then summarize the scope and the contributions of our work and provide the outline of the rest of the thesis.

1.1 Overview of power system reliability

The primary function of electric power systems is to supply electricity to all customers at all times and at an acceptable degree of quality. As such, reliability is an integral requirement in order for power systems to perform their primary function. The occurrences of several major blackouts in North America, such as the 1965 Northeast Blackout, led to the formation of the North American Electric Reliability Corporation (*NERC*) in response to the federal government's position that "electric reliability was too important to be left to anyone but the federal government." *NERC* is a not-for-profit entity that consists of eight reliability councils as illustrated in Fig. 1.1. *NERC* and its constituent councils develop and enforce reliability standards, perform annual assessments of short- and long-term reliability and monitor the bulk power system subject to oversight by the Federal Energy Regulatory Commission (*FERC*) and governmental authorities of Canada.

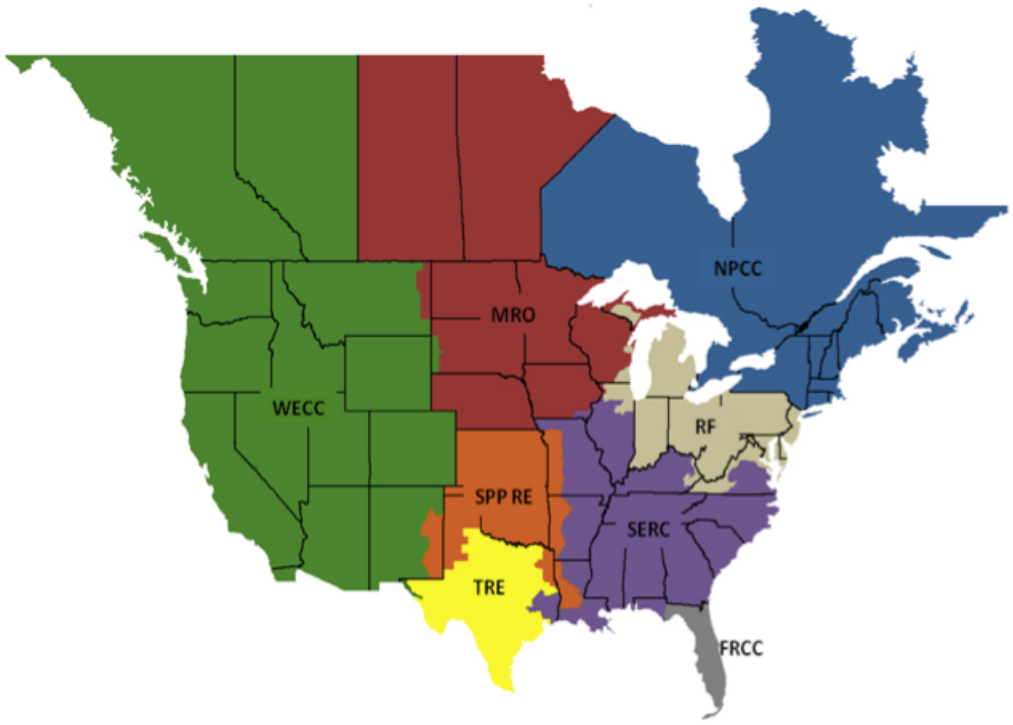

Figure 1.1: *NERC* reliability councils.

In this thesis we use the definition of power systems reliability given by *NERC*: the degree of performance of the bulk electric system that results in electricity being delivered to customers within accepted constraints and in the amount desired [1]. *NERC* further characterizes the bulk power system reliability with two complementary but independent concepts, adequacy and security. Adequacy is a measure of the system ability to provide adequate generation to meet all its firm load obligations. In other words, adequacy is related to the existence of sufficient generation resources in the system to meet consumer demand. Security describes the system ability to withstand sudden disturbances occurring in that system. In order to understand the distinction between the two concepts, we may view adequacy as the area that relates to the long-term evaluation of a static requirement: the total installed capacity that the system must plan and construct in advance in order to ensure adequate supply of future demand. On the other hand, security relates to maintaining sufficient commited capacity that can be dispatched within specified short periods — usually in a timescale of seconds to hours — during actual system operations so as to overcome the impacts of various contingencies, when and if they occur. Both these areas must be examined

in the planning regime for the evaluation of alternative generation facilities; however, once the decision has been made, the short-term security requirement becomes an operational problem. In this work our focus is entirely on the resource adequacy component of bulk power system reliability.

The quantification techniques adopted to perform resource adequacy assessment studies range from analytical to simulation approaches to address the requirements of the particular study. Such studies involve the prediction of the capability of the system to meet the inherently uncertain future load with all other sources of uncertainty explicitly represented. Therefore, in resource adequacy assessment it is impossible to predict exact figures, and statements about future events can be made only in terms of averages or the likelihood of various alternative possibilities. As such, the various approaches and metrics for facilitating resource adequacy predictions and setting appropriate criteria are typically probabilistic in nature.

In resource adequacy assessment studies at the bulk power system, the two sources of uncertainty typically considered are the loads and the supply resources, with the transmission network assumed to be 100 % available. In this context, all supply resources are considered, including conventional fossil-fired and nuclear units, RRs as well demand response resources (DRRs). The latter refer to loads capable to adjust their consumption in response to price signals that provide incentives to curtail consumption and allow loads to actively participate in ensuring demand-supply equilibrium. In the traditional resource adequacy evaluation framework the supply resources are, typically, represented as multi-state components where each state has an associated probability of occurrence. The system loads are represented by a probability distribution obtained from the chronological load curve, i.e., the system load values for a given time period and time resolution. The probabilistic models for the loads and supply/demand resources are combined in the resource adequacy evaluation framework to compute the metrics of interest. A key aspect of the framework is that it requires the specification of the smallest time granularity in the load representation with the fundamental assumption that uniform system conditions hold throughout each unit of time, i.e., constant values of loads and static capacity states for the supply resources. As such, the framework lacks the ability to incorporate time-varying phenomena since the time element has been abstracted out in the load and supply resource representations.

The resource adequacy metrics computed from the framework — and the most widely adopted in the industry — are the loss of load probability ($LOLP$), the loss of load expectation ($LOLE$), the loss of load hours ($LOLH$) and the expected unserved energy (EUE). The principal use of such metrics is in planning studies to allow for the side-by-side comparison of different alternative resource mixes to meet the forecasted electricity demand over a specified period of time. Resource adequacy metrics are also defined for studies where the failures in the components of the transmission network are taken into consideration. Examples of such metrics include the probability of load curtailments (PLC), the expected frequency of load curtailments ($EFLC$), expected demand not supplied ($EDNS$), the bulk power interruption index ($BPII$) and others. In addition, several resource adequacy metrics are defined solely for the distribution system such as the system average interruption frequency index ($SAIFI$), system average interruption duration index ($SAIDI$) or the customer average interruption frequency index ($CAIFI$).

The resource adequacy metrics are frequently used to set appropriate criteria or standards to determine the boundary between the acceptable or adequate outcomes and those that are not. For example, the utility industry and practitioners have adopted for years the industry-wide "1 day in 10 years" criterion, which requires that electric power systems maintain sufficient generation capacity and DRRs so that the event that the system peak load exceeds the system available supply occurs only once in a 10-year period. Although it is not set as the *de jure* reliability standard, the "1 day in 10 years" is so well-entrenched in the industry that it has become a *de facto* minimum accepted level of resource adequacy in North America. The "1 day in 10 years" criterion can be traced back to at least 1947 in a paper written by G. Calabrese [2], although the precise origin of the criterion is not known with certainty. Many discussions in regulatory, industry and various technical forums focus on the appropriateness of such reliability criteria for resource adequacy studies in the rapidly changing electricity industry. The main questions raised center on the definitions of resource adequacy metrics and criteria, their interpretation and the implementation requirements to comply with $NERC$ standards. Such discussions make evident that there persists a lack of clarity in the meaning of the "1 day in 10 years" criterion as well as in the underlying assumptions made in the resource adequacy metric evaluations. As a result, there co-exist multiple interpretations of the met-

rics and standards, which make it very challenging to meaningfully compare resource adequacy across different power systems [3]. In addition, the continual changes in the resource mix brought about by the deeper penetrations of intermittent generation, introduce new challenges to resource adequacy studies and have led to even wider disparities in resource adequacy assessment in the power industry.

1.2 Motivation

Resource adequacy assessment studies and the evaluation of the associated metrics — *LOLP*, *LOLE*, *EUE* — are an integral part of the planning regime in electric utilities and grid operators to ensure that the system maintains sufficient supply/demand resources to meet the future demand. However, it is unfortunate that, as yet, there is no uniformity in the definition, evaluation methodology and use of the above adequacy metrics. In many cases, *LOLP* and *LOLE* are used interchangeably, and often resource adequacy criteria are expressed in terms of the *LOLP* metric without considering the appropriate assumptions in its computation. As such, there is an acute need for a comprehensive and consistent resource adequacy assessment framework that is no longer subject to misinterpretations. Such a framework can be the vehicle to clarify the ambiguities between the various interpretations of the resource adequacy metrics and criteria adopted in the electricity industry. Furthermore, the various policy initiatives that call for higher integrations of *RR*s [4]-[5], introduce new challenges to resource adequacy studies due to the distinct time-varying, intermittent and uncertain nature of the *RR*s. For example, while unscheduled or *forced* outages [6] in conventional resources are, typically, due to various failures, renewable technology resources — although characterized by high availability — can only generate electricity when the fuel is available, e.g., the wind blows within acceptable ranges. Hence, the static representation of *RR*s [7]-[8] in the conventional, time-abstracted resource adequacy framework is unable to appropriately represent their time-varying output as well as their temporal correlations.

A conventional generator's capacity contribution to resource adequacy has been traditionally approached by the concept of the effective load carrying capability (*ELCC*) [9], which generally represents the additional load in *MW*

that can be served by the generator at a designated reliability target. More specifically, a generator contributes to resource adequacy if it reduces the $LOLE$ ($LOLH$) in some or all days (hours) [10]. For RRs, the capacity contribution is a function of the time of delivery and the reductions to $LOLE$ that would be achieved with that resource. Because $LOLE \simeq 0$ ($LOLH \simeq 0$) during most days (hours), a resource can contribute to adequacy if it generates during times where $LOLE \neq 0$ ($LOLH \neq 0$). This implies that if a renewable resource generates little power during these times, it will have a low capacity contribution to resource adequacy although it may produce significant amount of energy during the rest of year. Non-zero $LOLE$ or $LOLH$ values may occur for example during the summer months when the load reaches or is close to its peak value. Solar generation resources are, typically, characterized by good tracking ability of the peak loads therefore resulting in a significant reduction of the $LOLE$. In such cases, the solar resource would have a capacity contribution close to its rated capacity. However, the presence of clouds and/or ozone haze may reduce the solar output during load peaks resulting in the resource's contribution to be significantly lower than its rated capacity. Therefore, in order to appropriately incorporate RRs in the resource adequacy assessment framework, we need to ensure that the chronological output data used from RR plants are time synchronized with the chronological load data. Such a requirement is necessary in order to capture the underlying weather correlation, as weather is the driver not only for the wind output but also for the load.

An alternative approach to assess RR generation capacity contributions to resource adequacy is based on the capacity factor evaluation during system critical periods, such as peak hours. The capacity factor of a resource is defined as the net electricity generated, for the time considered, to the energy that could have been generated at continuous full-power operation during the same period. The capacity factor evaluation approach entails two steps: first, a time period for the system in question is defined — typically a number of hours during system peak load for summer and winter — and second, the average output of the variable resource is calculated over that period. The advantage of this approach lies in its simplicity, while studies have also shown that it has a reasonably accurate performance [11]-[12]. Such studies demonstrate that a good approximation of the wind $ELCC$ is possible but it depends on the number of hours and the method that these hours are

selected for the time period. Capacity factor methods are widely adopted by many independent system operators (*ISO*s) and regional transmission organizations (*RTO*s) in North America, including *PJM*, *ISO-NE*, *NYISO*, *CAISO*[1] and others. In Table 1.1 we present the various methods employed to evaluate wind generation resource capacity contributions across various *ISO*s/*RTO*s.[2]

Table 1.1: Wind capacity contribution evaluation methods in *ISO*s and *RTO*s in North America.

region	method	comments
PJM	peak period	average capacity factor for hours 3-6 PM, June-Aug
NYISO	peak period	summer capacity credit for hours 2-6 PM, June-Aug and winter capacity credit for hours 4-8 PM, Dec-Feb in previous 5 years
ISO-NE	peak period	capacity credit is median net output from 2-6 PM, June-Sep in previous 5 years
MISO	*ELCC*	analyses indicate a capacity contribution at 8% of rated capacity
CAISO	peak period	for a 3-year period, plant output that equals or exceeds 70% of hours 4-9 PM, Jan-March and Nov-Dec and hours 1-6 PM, April-Oct
ERCOT	*ELCC*	wind generation is included with 8.7% of nameplate capacity
SPP	peak period	assigns monthly wind capacity value as 85^{th} percentile of wind generation during top 10% of load hours with 10 years of data

The appropriate incorporation of *RR*s in resource adequacy studies requires the careful consideration of the impacts that such resources may have on the profile of the system net load, i.e., the load that must be served from conventional generation. More specifically, when *RR*s are integrated to the

[1]Pennsylvania-New Jersey-Maryland Interconnection (*PJM*), *ISO* New England (*ISO-NE*), New York *ISO* (*NYISO*), California *ISO* (*CAISO*).

[2]The data presented in Table 1.1 are acquired from [10]. The *ISO*s/*RTO*s referred in the table include also the Midcontinent *ISO* (*MISO*), the Electric Reliability Council of Texas (*ERCOT*) and the Southwest Power Pool (*SPP*).

resource mix, it is possible that both the time and magnitude of the daily net peak load may change. In Fig. 1.2 we illustrate the net load for a typical summer day in the New York Control Area (*NYCA*) for increasing levels of solar generation penetration [13]. From the diagram it can be seen that as solar generation penetration deepens, the daily peak load magnitude decreases but also shifts from 5 PM in the afternoon to 7 PM in the evening. For relatively low *RR* penetrations such effects may not be a significant issue. However, as the integrations of renewable technology resources increase, a resource adequacy evaluation framework that does not consider time-synchronized load and *RR* data, may be limited in its ability to capture the actual risk of the system to meet its future demand. As such, the assessment of the impacts

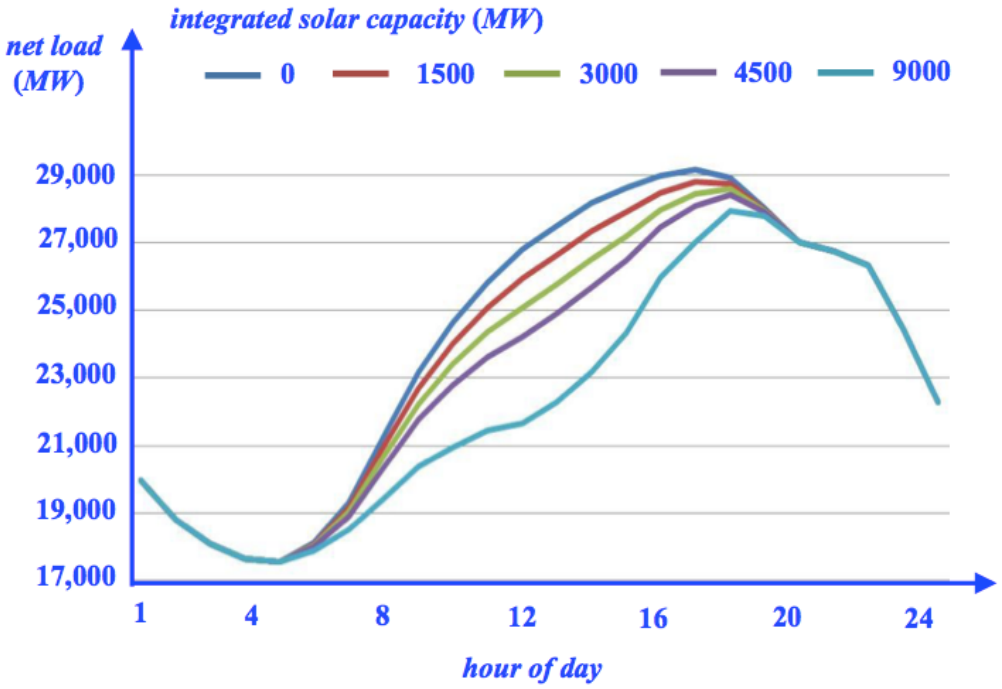

Figure 1.2: Net load for *NYCA* in a typical summer day and for different levels of solar penetration.

of the changes in *RR* penetrations on the grid's resource adequacy becomes an acute necessity. *NERC* has repeatedly called for adequacy studies that "provide ongoing evaluation of the potential impacts of the new variable generation on th grid" [10]. Significant contribution in this direction is the study presented in [14]. With data of up to 10 years of wind outputs for the Irish power system, the authors evaluate the *ELCC* for wind and analyze the effects of the number of wind farms, the data time period and time

resolution on the wind capacity contribution. Similar studies on the capacity contribution of solar resources are presented in [15]. However, all these studies fail to assess the impacts of deepening *RR* penetrations on the widely adopted resource adequacy metrics. Such studies are critically important in order to allow meaningful comparisons among the metrics, shed light on the requirement for additional new metrics and contribute to the *NERC*'s vision for "more widely adopted energy-related reliability metrics and targets as the share of variable generation increases in the power systems." This thesis directly addresses all the issues discussed in the incoporation of *RR*s in resource adequacy studies and reports on the development of a comprehensive framework that appropriately models the time-varying and intermittent nature of such resources to evaluate their capacity contributions.

1.3 Scope and contribution of the thesis

In this thesis, we initially discuss the traditional resource adequacy evaluation framework to define the industry-wide metrics and to address a broad range of inconsistencies associated with the metrics interpretations. We pay special attention on the underlying assumptions in the metrics evaluation and clarify the ambiguity between the mulitple interpretations of the "1 day in 10 years" criterion. The usefulness and physical relevance of the criterion are out of the scope of this thesis and consequently are not investigated. The limitations of the traditional resource adequacy assessment approach to represent the intermittent and time-varying nature of *RR*s lead us to the development of a stochastic simulation-based framework for adequacy studies in systems with integrated *RR*s. In the simulation-based framework, the system loads and supply/demand resources are modeled as discrete-time random processes (*r.p.*s), whose distribution have no analytical characterization. Indeed, the framework uses past historical load, conventional unit availability and solar/wind data to construct the sample paths (*s.p.*s) of the *r.p.* representations. A salient aspect of the *r.p.* representation is the explicit consideration of the spatial and chronological correlations among the *s.p.*s of the loads and supply/demand resources. The evaluation approach makes use of Monte Carlo simulation techniques [16] for the efficient sampling of the *r.p.*s in order to generate realizations of the outputs of the resources

and loads from which the resource adequacy metrics are evaluated for each simulation run.

The implementation of the proposed framework provides the ability to facilitate the computation of additional metrics that the resource adequacy studies require to further characterize the impacts of the deepening RR penetrations. In this thesis, we are particularly interested to study the marginal behavior of the resource adequacy metrics with respect to the deepening RR penetrations. As such, we define and evaluate appropriate sensitivity indices to quantify the impacts of RR penetrations on the metrics of interest. The new indices effectively capture the marginal behavior of the adequacy metrics and provide valuable insights to grid operators and planners of how each category of RRs affects each metric in particular. Furthermore, the framework allows for the evaluation of resource adequacy metrics for data even with different time resolutions. Another useful application of the proposed scheme is for the computation of the $ELCC$ of each RR. More specifically, to obtain the $ELCC$ of a particular RR unit, multiple applications of the framework can be performed to obtain the resource adequacy metrics with and without the integrated RR. The $ELCC$ of the RR can be evaluated as the additional conventional generation capacity to attain the same resource adequacy metric with the RR unit integrated into the grid.

A significant aspect of the thesis is the broad range of applications of the proposed framework to study both the short and longer time-periods for planning, operations and other purposes. As such, we perform extensive studies to quantify the impacts of the deepening RR penetrations on the resource adequacy of large-scale grids. The distinct impacts of such penetrations have not been quantified so far in the way performed in the studies. Furthermore, the study results provide important information on the care that grid operators must exercise in order to schedule the retirement of conventional fossil-fired generation resources so as to maintain the "1 day in 10 years" criterion. More specifically, our analysis provides a comprehensive quantification of the limiting nature of the replacement of controllable resources by RRs as well as the level of conventional resource retirement for a specific addition of RR facility. The studies we perform aim to promote a better understanding of the impacts of renewable generation resources on system resource adequacy and their interaction with conventional resources.

The scope of our discussion in this thesis is limited to resource adequacy

studies at the bulk power system with both supply and demand-side resources considered. The transmission network is assumed everywhere to be 100 % available and congestion-free. The resources at the distribution level are implicitly incorporated via the load demand. Our focus is only on wind and solar *RR*s with pumped-storage hydro generation assumed constant for each wind and solar penetration scenario. Furthermore, in this thesis we do not consider how reliable the system and its various subsystems should be. This is a vitally important question that cannot have a simple answer because different systems, utilities and customers have different requirements and expectations.

This thesis consists of four additional chapters and four appendices. In Chapter 2, we start out with the discussion of the traditional resource adequacy assessment framework and provide the analytical setting for the consistent evaluation of the *LOLP*, *LOLE*, *LOLH* and *EUE* metrics. In Section 2.4 of this chapter we introduce the stochastic simulation-based resource adequacy evaluation framework with the capability to represent the time-varying nature of loads and supply/demand resources. We further present the step-by-step computational procedure to evaluate the resource adequacy metrics in the simulation-based framework.

In Chapter 3 we provide the technique with which we incorporate *RR*s in the simulation-based framework and discuss the impacts of deepening *RR* penetrations in the grid's resource adequacy. We further define additional sensitivity indices to capture the marginal behavior of the metrics with respect to deepening renewable penetrations and to investigate the substitutability of *RR*s to conventional resources.

In Chapter 4, we provide a brief description of the study system and discuss the nature and scope of the application studies of the simulation-based resource adequacy framework. We present the results of two representative sets of studies on the system. One with integrated wind and solar *RR*s together with the existing fleet of conventional resources and a second with the gradual replacement of the conventional resources by renewable generation capacity. For each study we analyze multiple scenarios of solar and wind generation penetrations to evaluate the resource adequacy metrics — the *LOLE*, *LOLH* and the *EUE* — and their associated sensitivities. The study results demonstrate the improvement in the grid's resource adequacy as the penetrations of *RR* deepen. Specifically, the results indicate the dis-

tinct nature of deepening solar and wind penetrations and their common diminishing marginal return characteristic. When the retirement of fossil-fired generation units is taken into account, it becomes clear that additional resources are needed to maintain the grid's ability to meet the industry-wide "1 day in 10 years" criterion. We provide in Chapter 5 a summary of the key findings in the work presented in this thesis. We also indicate directions for future research in the topic.

CHAPTER 2

RESOURCE ADEQUACY FRAMEWORKS

In this chapter we start out our discussion of resource adequacy with a focus on conventional generation resources. A fundamental concept in resource adequacy studies is the loss of load event, whose mathematical characterization is key in the quantification of resource adequacy. Indeed, it becomes the basic building block in the definition and evaluation of various resource adequacy metrics used for adequacy measurements. Our discussion includes a review of the analytical resource adequacy evaluation framework. We use the framework to explain the significance and the salient characteristics of the industry-wide resource adequacy metrics and to clarify various misconceptions associated with their interpretation. Specifically, we provide an unambiguous definition of the widely used "1 day in 10 years" resource adequacy criterion. Furthermore, we point out the key limitations of the framework as it cannot accommodate the evaluation of resource adequacy for systems with time-varying resources.

The limitations of the analytic framework are addressed through the construction of a more general, simulation-based framework that can be used for the resource adequacy analysis for systems with time-varying resources. Such a framework can in particular be used for resource adequacy evaluation of systems with integrated *RR*s. A key element of this more general framework is the ability to represent in as much detail possible the conventional generation resources and provide the basis for the definitions of the analogues of the industry-wide resource adequacy metrics. The chapter provides the entire analytical basis for the work presented in this thesis.

2.1 Resource adequacy

Resource adequacy is defined as the ability of the electric system to supply the aggregate electrical demand and energy requirements of the end-use customers at all times, taking into account scheduled and reasonably expected unscheduled outages of system elements [1]. In this context, a scheduled outage is an outage that results when a system component is deliberately taken out of service at a planned time and for a specified duration, typically, for purposes of construction, preventive maintenance or repair. An unscheduled or *forced* outage is an outage that results from emergency conditions created by a component, that require the component be taken out of service immediately, either automatically or as soon as the appropriate switching operations can be performed, or an outage caused by improper equipment operation or human error [6]. We point out the difference between a component outage and a power shortage or interruption. An outage, be it scheduled or forced, refers to the state of a component when it is not available to perform its intended function due to the occurrence of some event directly associated with that component. On the other hand, power shortages or interruptions describe a situation where the firm load obligations of the system exceed the instantaneous available generation capacity and consequently result in the curtailment of firm electricity supply to load customers.[1] We refer, typically, to such situations as loss of load ($\ell.o.\ell.$) events.

In general, a $\ell.o.\ell.$ event is caused by one or more component outages, but a component outage need not result in a $\ell.o.\ell.$ event. A $\ell.o.\ell.$ event will occur only when the system load exceeds the total available generation capacity. Resource adequacy assessment examines the $\ell.o.\ell.$ events to evaluate the probability of such events over a specified period of time. In this thesis, we focus on resource adequacy of the bulk power system — the high voltage transmission, generation and the load resources connected at that level — to determine the ability of system resources to meet the forecasted demand. The system resources considered include fossil-fired and nuclear units,

[1]Most customer interruptions of service are due to distribution network events, such as a squirrel, who seeks to have a warmer environment and enters into a transformer and ends up electrocuted. Such events may lead to customer outages due to a failure in the distribution system. Although more frequent, such failures have more localized effects than outages in the bulk power system. In this thesis, we focus on the failures only in the generation resources as they affect large portions of the system and therefore can have widespread consequences for both society and the environment.

RRs and demand response resources (DRRs). In resource adequacy studies, we assume that the transmission network is capable to deliver energy from any generation source to any load location without losses, congestion or bus deterioration. Moreover, we ignore other parts of the system, such as the distribution. In conclusion, resource adequacy assessment entails the evaluation of the probabilities associated with $\ell.o.\ell.$ events, within a framework of well-defined and appropriate assumptions.

2.2 The time-abstracted framework

Resource adequacy is one of the most important issues in planning studies and, various studies are carried out for different duration periods that can last from days to years. The goal of such studies is to assure that the planned future system can adequately meet customers' future load and energy needs. Therefore, the nature of the problem considered is inherently uncertain as it requires the prediction of future phenomena and behavior of the system. The main sources of uncertainty typically considered are the variations in system loads and the available capacity of the supply resources. The bulk power system load — the sum of the nodal loads — exhibits wide fluctuations in a given period due to customers' variations of electricity usage, changes in weather conditions, economic factors, government policy decisions, and other drivers. Also, the uncertainty related with the available capacity of supply resources at a future time, needs to be explicitly taken into account in resource adequacy assessment studies. For example, conventional generation resources, such as coal, nuclear and gas units, experience forced outages due to various causal factors that result in a unit's ability to provide only part or zero of its capacity. Consequently, a resource adequacy evaluation framework requires the explicit and appropriate representation of the wide range of sources of uncertainty in the bulk power system.

The time-abstracted framework is an analytical construct for resource adequacy assessment that integrates the models of the load and supply resources and the computational schemes for the adequacy evaluation and the metrics of interest. The fundamental assumptions under which we construct the framework are:

$A\,1$ The only sources of uncertainty considered are in the system loads and

supply resources.

$A\,2$ The uncertainty in the loads is independent of that in the supply resources.

$A\,3$ The failures/repairs of the system supply resources occur independently of each other.

At the outset, we define the smallest indecomposable unit of time, i.e., the resolution of time used, which is typically study-dependent. The framework is used to perform a study over a given period $\mathscr{T}$, usually specified as a set of hours or days. Hourly (daily) time resolution implies that the smallest indecomposable unit of time is one hour (day) and no phenomena of shorter duration can be represented. For hourly time resolution, we denote by $\mathscr{T}_h$ the study period represented by the set that consists of all the H hours in $\mathscr{T}_h = \{h : h = 1, 2, \ldots, H\}$. For a daily resolution, $\mathscr{T}_d$ is represented by the set that consists of all the D days in $\mathscr{T}_d = \{d : d = 1, 2, \ldots, D\}$. As an example, we show in Fig. 2.1 a study period of one week whose $\mathscr{T}_h$ consists of 168 non-overlapping hourly subperiods and so $\mathscr{T}_h$=$\{h : h = 1, 2, \ldots, 168\}$. For a daily resolution, the same one-week period consists of seven non-overlapping such periods, one for each day of the week and, consequently $\mathscr{T}_d$=$\{d : d = 1, 2, \ldots, 7\}$. Throughout this thesis, we limit the time resolution to either one hour or one day.

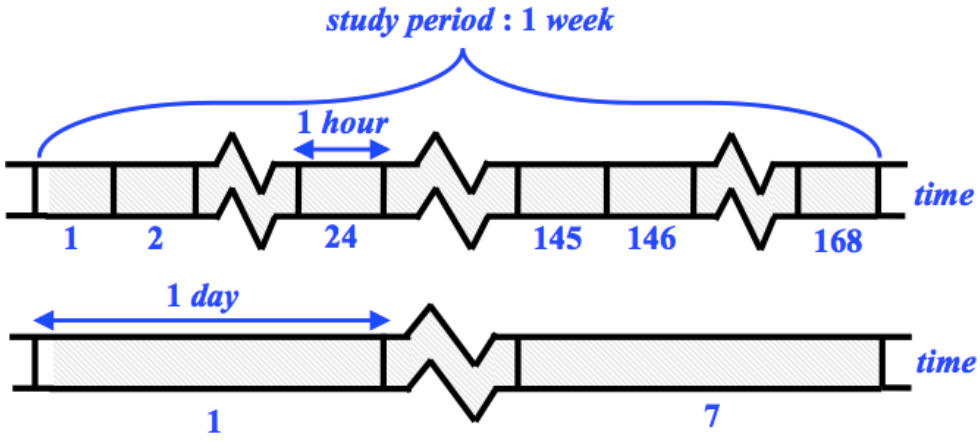

Figure 2.1: Hourly and daily representation of a one-week study period.

Once the time resolution is specified, we delve into the modeling of loads and supply/demand resources. We represent probabilistically the uncertainty

associated with the system load, which we think as a random variable ($r.v.$) denoted by $\underset{\sim}{L}$. The time resolution provides the basis for the appropriate representation of the loads. Under hourly resolution, the sample space of the load $r.v.$ is the set of hourly values given by $\{\ell_h : h \in \mathscr{T}_h\}$. Each load value ℓ_h is, in fact, a snapshot of the system load at hour $h \in \mathscr{T}_h$ and, under the stated assumptions the "fixed" load over the entire hour. Such an hourly value represents the sum of all the loads in the bulk power system for that hour. Under the daily time resolution, the sample space of $\underset{\sim}{L}$ is given by $\{\ell_d : d = 1, 2, \ldots, D\}$ with each ℓ_d as the daily peak load. Under the stated assumptions, for the daily resolution, the system demand is represented by the peak hourly value of each day. Once the demand values under an hourly resolution are known, the values ℓ_d, $d \in \mathscr{T}_d$ are computed directly from the set $\{\ell_h : h \in \mathscr{T}_h\}$ using

$$\ell_d = \max\left\{\ell_{24(d-1)+1}, \ell_{24(d-1)+2}, \ldots, \ell_{24d}\right\}, \tag{2.1}$$

where $\ell_{24(d-1)+h}$ represents the load value at hour h of day d. We observe that such a representation implies, in effect, an upper bound for the actual load in the system as the peak load is experienced only during the peak load hour(s). We illustrate the hourly and daily representations for a one-week study period in Fig. 2.2. For the hourly resolution, the total load is represented by the 168 hourly values. The daily peak values are indicated by the broken lines and the daily resolution model is shown.

We develop a probability distribution of $\underset{\sim}{L}$ from the hourly load curve for the given period: if we ignore time, we can rearrange the loads in order of decreasing values from the highest to the lowest and construct the load duration curve (LDC). Figure 2.3 illustrates the LDC curve for the demand given in Fig. 2.2, with the time axis normalized to have 168 hours equal to 100 percent. Note that such a reordering involves complete loss of all ideas related to time and so the chronological order of loads in the period is no longer available. Every point (t, ℓ) on the LDC represents the percentage of time t that load exceeds the given value ℓ. We interpret this fraction of time as the probability that load exceeds the value ℓ.

We next consider the representation of the conventional generation resources in the supply system that consists of G such resources and we denote them as $\mathscr{G} = \{g_k : k = 1, 2, \ldots, G\}$. Each $g_k \in \mathscr{G}$ denotes a generation plant

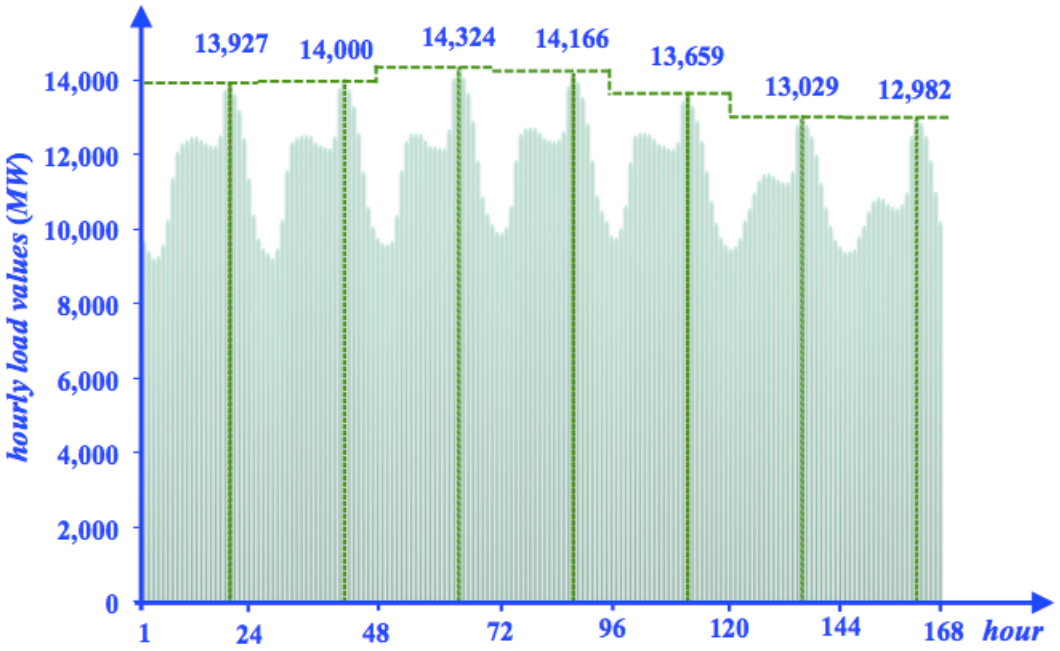

Figure 2.2: Example of the system loads for a week under hourly resolution. Each peak hour is indicated by the bold broken line and is used to construct the load values under daily resolution.

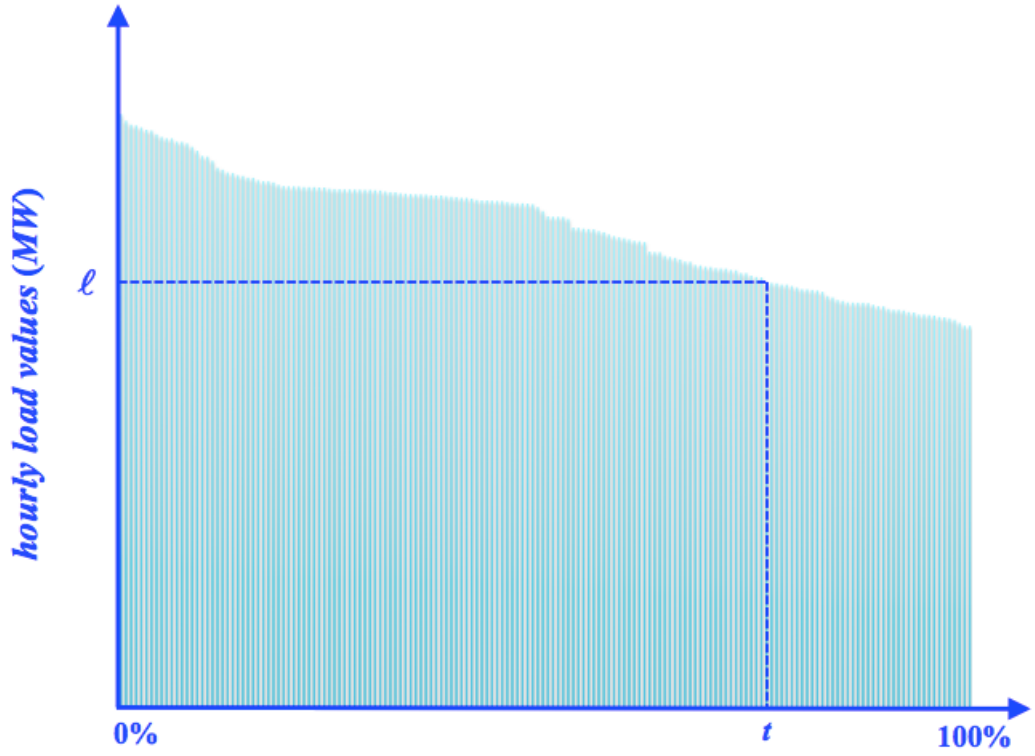

Figure 2.3: Load duration curve with normalized time axis.

that may consist of a single or a block of units and from now on we will use the term unit to refer to any such generation plant. We model each conventional unit by a multi-state *r.v.*, whose states represent the discrete capacity values of the unit, from total unavailability — the unit is fully outaged — to full capacity. Each state has an associated probability and at any point in time the unit can be in only one of its possible states. The state probabilities are the long-run probabilities determined from the steady-state behavior of the unit and are independent of time [6]. Furthermore, each generation unit's model satisfies the assumption of uniform representation of the supply system for the entire simulation period. In effect, the model of each generation unit is time independent with the time abstracted out. Mathematically, the model of each $g_k \in \mathscr{G}$ with n states, in terms of the available capacity *r.v.* $\underset{\sim}{A}_k$ is given by

$$\underset{\sim}{A}_k = \begin{cases} c_k, & \textit{with probability } p_k \\ d_k^1 & \textit{with probability } r_k^1 \\ d_k^2 & \textit{with probability } r_k^2 \\ \vdots & \\ d_k^{n-2} & \textit{with probability } r_k^{n-2} \\ 0 & \textit{with probability } 1 - \sum_{j=1}^{n-2} r_k^j - p_k \ . \end{cases} \tag{2.2}$$

The expression in (2.2) describes the probability mass function (*p.m.f.*) of the *r.v.* $\underset{\sim}{A}_k$. The sum $\sum_{k=1}^{G} \underset{\sim}{A}_k$ represents the total system available capacity *r.v.*, which we denote by $\underset{\sim}{A}_T$. Its distribution can easily be derived from the *p.m.f.*s of the statistically independent *r.v.*s $\underset{\sim}{A}_k$ in the sum [17]. The statistical independence assumption is reasonable given the fact that the conventional units are put in service at different times, have different outages and may have different generation technology implemented. The number of states of $\underset{\sim}{A}_T$ is J, which may be a very large number for a large value of G. Each state corresponds to a distinct[2] configuration of available capacity

[2]The states of $\underset{\sim}{A}_T$ need not have distinct values since multiple configurations of the individual states of the units may result in the same total available capacity a_j, $j = 1, 2, \ldots, J$. In such cases, we can merge states with the same a_j to determine the probability as the sum of the merged states' respective probabilities.

that we denote by a_j for $j = 1, 2, \ldots, J$. Every state a_j has an associated probability denoted by p_j.

The resource adequacy quantification entails the evaluation of the probability of a $\ell.o.\ell.$ event over a specified period $\mathscr{T}_h$ or $\mathscr{T}_d$. From this point on and without any loss of generality, we assume hourly time resolution unless we explicitly state otherwise. The probability of a $\ell.o.\ell.$ event, which we refer to as loss of load probability ($LOLP$), is defined as the probability of the event that load exceeds the total available capacity [17] and is mathematically expressed by

$$\rho = \mathbb{P}\left\{ \underset{\sim}{A}_T < \underset{\sim}{L} \right\} \ . \tag{2.3}$$

Here we use ρ to denote the $LOLP$ and $\mathbb{P}\{\cdot\}$ to denote probability. To evaluate the expression in (2.3) we make use of the convolution formula and of assumption $A\,2$. Then for $\forall\ x \in \mathbb{R}$,

$$\begin{aligned} F_{\underset{\sim}{A}_T - \underset{\sim}{L}}(x) = \mathbb{P}\left\{ \underset{\sim}{A}_T - \underset{\sim}{L} \leq x \right\} = \mathbb{P}\left\{ \underset{\sim}{A}_T \leq \underset{\sim}{L} + x \right\} \\ \int_{-\infty}^{+\infty} \mathbb{P}\left\{ \underset{\sim}{A}_T \leq \ell + x \ \middle| \ \underset{\sim}{L} = \ell \right\} f_{\underset{\sim}{L}}(\ell)\ d\ell = \\ \int_{-\infty}^{+\infty} \mathbb{P}\left\{ \underset{\sim}{A}_T \leq \ell + x \right\} f_{\underset{\sim}{L}}(\ell)\ d\ell = \int_{-\infty}^{+\infty} F_{\underset{\sim}{A}_T}(\ell + x) f_{\underset{\sim}{L}}(\ell)\ d\ell \ . \end{aligned} \tag{2.4}$$

In expression (2.4), $f_{\underset{\sim}{L}}(\ell)$ denotes the probability density function ($p.d.f.$) of demand and $F_{\underset{\sim}{A}_T}(\cdot)$ the cumulative distribution function ($c.d.f.$) of the total system available capacity. We devote Appendix A to provide a detailed discussion of the analytical details in the computation of ρ for a study period $\mathscr{T}_h$, which we denote by $\rho_{\mathscr{T}_h}$.

The $LOLP$ for a period $\mathscr{T}_h$ is evaluated as the weighted sum of the $LOLP$ values for each demand level ℓ_h. The mathematical expression of $LOLP$ is given in (A.6), which we repeat here to facilitate our discussion:

$$\rho_{\mathscr{T}_h} = \frac{1}{H} \sum_{h=1}^{H} \phi(\ell_h) \ . \tag{2.5}$$

We can similarly derive the $LOLP$ for a period $\mathscr{T}_d$ where the smallest time granularity is one day. The evaluation procedure is essentially analogous to the hourly resolution approach. The key difference is that, in the daily

representation we condition on the event of being in any of the D days in the period and each load value ℓ_d represents a daily peak load. We note that the order in which the probability computations are performed in either scheme, is not of impact to the determination of ρ. Each $\phi(\ell_h)$ or $\phi(\ell_d)$ simply represents a term in the summation and the order of the term in the addition is irrelevant in the evaluation of the $LOLP$ for the entire period. Therefore,

$$\rho_{\mathscr{T}_d} = \frac{1}{D} \sum_{d=1}^{D} \phi(\ell_d) \ . \tag{2.6}$$

From the previous discussion we conclude that resource adequacy is related to the idea of a $\ell.o.\ell.$ event and its probability of occurrence — the $LOLP$. The definition of the $LOLP$ encompasses two key sources of uncertainty: the system loads and the supply/demand resources. In order to correctly interpret the $LOLP$, it is critical to clarify the time resolution and the length of the evaluation period. The value of the $LOLP$ by itself provides incomplete information on the system resource adequacy absent the specification of such underlying assumptions in its evaluation. In general, the $LOLP$ depends on a number of additional other factors such as the demand that the supply resources must meet, the total number of generation units in the supply system as well as their availability states and their associated probabilities.

2.3 Resource adequacy metrics

With the developed mechanisms and the framework to evaluate the $LOLP$, we proceed with the discussion of industry's widely used resource adequacy metrics. We make detailed use of the analysis presented for the $LOLP$ computation, which we view as the basic building block for the computation of each of the resource adequacy indices of interest. We begin our discussion with the evaluation of $LOLP$ for a time resolution of a day and a study period $\mathscr{T}_d$. The $LOLP$ metric calculated under such assumptions is also frequently referred to as the loss of load expectation ($LOLE$). The $LOLE$ index for a specified period, is defined, as the expected number of days with a $\ell.o.\ell.$ event, under the explicit assumption that each day's load is represented by its daily peak value. The $LOLE$ measures the mean number of $\ell.o.\ell.$ events in the specified period $\mathscr{T}_d$ and is expressed as *number of events* per *number*

of days in $\mathscr{T}_d$. In order to gain more insights into the meaning and interpretation of the *LOLE*, we present an alternative procedure to evaluate the *LOLE*. We note that the *LOLE* value equals the *LOLP* value for the period. We define the binary-valued *r.v.* $\underset{\sim}{M}_d$ for each day $d \in \mathscr{T}_d$ as

$$\underset{\sim}{M}_d = \begin{cases} 1, & if\ \ell.o.\ell.\ occurs\ in\ day\ d \in \mathscr{T}_d \\ \\ 0, & otherwise\ \cdot \end{cases} \tag{2.7}$$

If ℓ_d is the peak load of day d, the probability of the value m of $\underset{\sim}{M}_d$ is given by

$$\mathbb{P}\left\{\underset{\sim}{M}_d = m\right\} = \begin{cases} \phi(\ell_d), & if\ m = 1 \\ \\ 1 - \phi(\ell_d), & if\ m = 0\ \cdot \end{cases} \tag{2.8}$$

Then, for the D-day period $\mathscr{T}_d$, the *LOLE* $\xi_{\mathscr{T}_d}$ is

$$\begin{aligned} \xi_{\mathscr{T}_d} = \mathbb{E}\left\{\sum_{d=1}^{D} \underset{\sim}{M}_d\right\} \frac{days}{D\ days} &= \sum_{d=1}^{D} \left[1 \cdot \phi(\ell_d) + 0 \cdot (1 - \phi(\ell_d))\right] \frac{days}{D\ days} \\ &= \sum_{d=1}^{D} \phi(\ell_d) \frac{days}{D\ days}\ \cdot \end{aligned} \tag{2.9}$$

We interpret $\xi_{\mathscr{T}_d}$ to be the expected number of days out of D days in which the *daily peak load* exceeds the total supply system available capacity. The *LOLE* index is simply the value of the long-run average of the number of days with a $\ell.o.\ell.$ event in the period $\mathscr{T}_d$ of D days. Since the smallest unit of time is a *day* and no fraction of a day can be represented, the *LOLE* index cannot measure neither the capacity shortfall to meet the load nor the duration of the $\ell.o.\ell.$ event. For each day d, the procedure evaluates whether or not the total available generation capacity in the system is able to meet the daily peak load. Each day d with a $\ell.o.\ell.$ event contributes to the *LOLE* the amount $\mathbb{P}\left\{\underset{\sim}{A}_T < \ell_d\right\}$ and a day without a $\ell.o.\ell.$ event does not impact its value.

The daily peak load representation, in the *LOLE* evaluation in (2.9), is

unable to capture the more realistic situation that the $\ell.o.\ell.$ event happens only in those hours of day d in which the hourly load exceeds the corresponding hourly system total available generation capacity. Hence, we need to use a finer resolution of one hour as the smallest indecomposable unit of time to do so. For such a representation, we examine independently — of each other hour — each hour in the period $\mathscr{T}_h$ to evaluate the probability of inadequate generation to meet demand. The $LOLP$ of a period $\mathscr{T}_h$ is, typically, referred to as the loss of load hours ($LOLH$) in order to distinguish its value from the $LOLE$ metric, which is determined with a time granularity of one day. More specifically, the $LOLH$ index is defined as the expected number of hours with an $\ell.o.\ell.$ event in a period $\mathscr{T}_h$. We define the binary-valued *r.v.* $\underset{\sim}{M}_h$ for each hour $h \in \mathscr{T}_h$

$$\underset{\sim}{M}_h = \begin{cases} 1, & if\ \ell.o.\ell.\ occurs\ in\ hour\ h \in \mathscr{T}_h \\ \\ 0, & otherwise\ . \end{cases} \tag{2.10}$$

For an H-hour period $\mathscr{T}_h$, the $LOLH$ $\eta_{\mathscr{T}_h}$ is

$$\eta_{\mathscr{T}_h} = \mathbb{E}\left\{\sum_{h=1}^{H} \underset{\sim}{M}_h\right\} \frac{hours}{H\ hours} = \sum_{h=1}^{H} \phi(\ell_h)\ \frac{hours}{H\ hours}\ . \tag{2.11}$$

We interpret $\eta_{\mathscr{T}_h}$ as the expected number of hours out of H hours in which the hourly load exceeds the system total available generation capacity. Since the smallest time unit is one hour, no fraction of the hour can be represented and no duration of the $\ell.o.\ell.$ event can be measured. For every hour $h \in \mathscr{T}_h$, we examine whether the total available generation capacity exceeds the demand ℓ_h for that hour. Every hour h that experiences a $\ell.o.\ell.$ event contributes to $\eta_{\mathscr{T}_h}$ the probability of the event $\mathbb{P}\left\{\underset{\sim}{A}_T < \ell_h\right\}$, while the hours with no $\ell.o.\ell.$ events have zero contribution to the $LOLH$. We note that $\xi_{\mathscr{T}_d}$ is a unitless quantity as is $\eta_{\mathscr{T}_h}$, since (2.9) and (2.11) are similar.

While the indices $\xi_{\mathscr{T}_d}$ and $\eta_{\mathscr{T}_h}$ are similar, there are important differences. It is incorrect to substitute 1 day by 24 hours in (2.9) to evaluate $\eta_{\mathscr{T}_h}$ due to the inability to represent any fractional unit of time less than one day. Indeed, there exists no *one*-to-*one* and *onto* mapping between $\xi_{\mathscr{T}_d}$ and $\eta_{\mathscr{T}_h}$. For a given daily period $\mathscr{T}_d$ and the corresponding hourly period $\mathscr{T}_h$, the

relationship that captures the behavior between the two indices is given by the following inequalities

$$\xi_{\mathscr{T}_d} \leq \eta_{\mathscr{T}_h} \leq 24\,\xi_{\mathscr{T}_d} \ . \tag{2.12}$$

The left inequality in (2.12) states that $\eta_{\mathscr{T}_h}$ is an upper bound for $\xi_{\mathscr{T}_d}$. Furthermore the right inequality in (2.12) states that $\eta_{\mathscr{T}_h}$ is bounded by $24\,\xi_{\mathscr{T}_d}$ for the period of evaluation. The equality $\eta_{\mathscr{T}_h} = 24\,\xi_{\mathscr{T}_d}$ holds only for the case where the load in each of the 24 hours of each day in $\mathscr{T}_d$ remains constant at its daily peak value. The equality $\xi_{\mathscr{T}_d} = \eta_{\mathscr{T}_h}$ holds when there is exactly one $\ell.o.\ell.$ event for each day in the entire study period and that event occurs for the single hour with the daily peak load value. We present the proof of the inequalities in (2.12) in Appendix B.

We note that we are not restricted to use only hourly or daily load representations and there may be multiple resource adequacy metrics defined and evaluated as we use coarser or finer time resolutions. Such flexibility also dictates the necessity to thoroughly understand both the nature and the implications of the modeling assumptions so as to allow the comparative study of resource adequacy indices for the same system on a meaningful and consistent basis.

The resource adequacy metrics discussed so far do not consider the severity of the $\ell.o.\ell.$ event. A metric that evaluates the sum of the average firm hourly load shed, expressed in MWh, is the expected unserved energy (EUE). The EUE metric measures the expected value of energy not served due to inadequate available generation capacity in the system that causes the $\ell.o.\ell.$ events in the period $\mathscr{T}_h$. We denote $u_{\mathscr{T}_h}$ the EUE for the period $\mathscr{T}_h$. We evaluate $u_{\mathscr{T}_h}$

$$\begin{aligned} u_{\mathscr{T}_h} &= \sum_{h=1}^{H} \mathbb{E}\left\{MWh \text{ not served in hour } h\right\} \\ &= \sum_{h=1}^{H} \mathbb{E}\left\{ MWh \text{ not served} \;\middle|\; \text{hour } h \right\} \mathbb{P}\left\{\text{hour } h\right\} \ , \end{aligned} \tag{2.13}$$

where, we condition on each equiprobable event of being in the hour h of the period $\mathscr{T}_h$. In order to evaluate $u_{\mathscr{T}_h}$ we first define the capacity deficiency

r.v.

$$\underset{\sim}{\Delta}_h = max\left\{0, \underset{\sim}{L} - \underset{\sim}{A}_T\right\} \ , \tag{2.14}$$

where the subscript h of $\underset{\sim}{\Delta}_h$ indicates the hourly resolution of the study period. We partition the sample space of $\underset{\sim}{\Delta}_h$ into two non-overlapping events: $\underset{\sim}{L} > \underset{\sim}{A}_T$ and $\underset{\sim}{L} \leq \underset{\sim}{A}_T$. To evaluate $u_{\mathscr{T}_h}$, we make use of conditional expectation and reduce the calculations to the sample space defined by the event $\underset{\sim}{L} > \underset{\sim}{A}_T$. In this way,

$$\begin{aligned}
u_{\mathscr{T}_h} &= H \cdot \mathbb{E}\left\{\underset{\sim}{\Delta}_h\right\} \\
&= H \cdot \mathbb{E}\left\{\underset{\sim}{L} - \underset{\sim}{A}_T \,\middle|\, \underset{\sim}{L} > \underset{\sim}{A}_T\right\} \mathbb{P}\left\{\underset{\sim}{L} > \underset{\sim}{A}_T\right\} + \\
&\quad H \cdot \mathbb{E}\left\{0 \,\middle|\, \underset{\sim}{L} \leq \underset{\sim}{A}_T\right\} \mathbb{P}\left\{\underset{\sim}{L} \leq \underset{\sim}{A}_T\right\} \\
&= H \cdot \sum_{h=1}^{H} \mathbb{E}\left\{\ell_h - \underset{\sim}{A}_T \,\middle|\, \ell_h > \underset{\sim}{A}_T\right\} \mathbb{P}\left\{\underset{\sim}{A}_T < \ell_h\right\} \cdot \mathbb{P}\left\{\underset{\sim}{L} = \ell_h\right\} \\
&= \sum_{h=1}^{H} \mathbb{E}\left\{\ell_h - \underset{\sim}{A}_T \,\middle|\, \ell_h > \underset{\sim}{A}_T\right\} \phi(\ell_h) \ .
\end{aligned} \tag{2.15}$$

The *EUE*, in principle, may also be calculated for a load model with daily resolution under the assumption that the daily peak load is used to represent load. The *EUE* augments the information provided by the *LOLE* and *LOLH* metrics as it provides a measure in MWh of the energy not met due to $\ell.o.\ell.$ events. We note that each $\ell.o.\ell.$ event in a period contributes to the $\xi_{\mathscr{T}_d}$ ($\eta_{\mathscr{T}_h}$) an amount equal to its respective probability. However, the contribution of a 100 MWh or 1,000 MWh loss is weighted by the respective probability of the $\ell.o.\ell.$ event to compute $u_{\mathscr{T}_d}$ ($u_{\mathscr{T}_h}$).

We use this analysis to gain some insights into the meaning of the widely used industry standard of "1 day in 10 years". This measure of adequacy is sometimes expressed as $\xi_{\mathscr{T}_d} = 0.1$ day/year or as $\xi_{\mathscr{T}_d} = 1$ day/10 years. The interpretation of the "1 day in 10 years" standard is that the electric system maintains adequate generation and *DRR*s such that the system peak load is likely to exceed the available capacity at most once in any ten-year period. A frequent misconception in the interpretation of the "1 day in 10 years" criterion is that it is equivalent to $\eta_{\mathscr{T}_h} = 24$ hours/10 years. Such inference may result from the misinterpretation of the term "1 day" in the criterion

to refer to the entire time period of one day. Given that a day consists of 24 hours, it is easy to deduce that "1 day in 10 years" corresponds to "24 hours in 10 years", which translates to $\eta_{\mathscr{T}_h} = 24$ hours/10 years. However, based on the discussion for the metrics evaluation in the previous sections, such statements are inaccurate. The evaluation of $\xi_{\mathscr{T}_d}$ in days/year is based on the conduction of repeated experiments where the time resolution is fixed and the load representation remains uniform throughout each experiment for the entire study period $\mathscr{T}_d$. The *LOLE* $\xi_{\mathscr{T}_d}$ is the long-run expectation of the dichotomous outcomes of each experiment under the daily peak load representation. We cannot use the value of $\xi_{\mathscr{T}_d}$ to derive information on the value of $\eta_{\mathscr{T}_h}$ since we lack the required level of detail in the load representations. The evaluation of each metric involves two similar albeit different in terms of the underlying assumption procedures. The assumptions in the evaluation framework require the careful interpretation of each metric with full consideration of the limitations imposed by the resolution level, i.e., the definition of the smallest indecomposable unit of time.

2.4 The time-dependent framework

In the time-abstracted framework discussed in the previous sections, we prespecified the smallest indecomposable unit of time and decomposed the entire study period into a set of non-overlapping such time-units. We further imposed the fundamental assumption that throughout each time-unit in the set, the system conditions are uniform and therefore no time dependence is represented in the study. Indeed, throughout each experiment performed for each hour $h \in \mathscr{T}_h$ or day $d \in \mathscr{T}_d$, the system load is fixed and the available generation is statically represented by a set of capacity states. As a result, the time-abstracted framework, lacks the capability to represent the time-dependent nature of the demand and supply resources, particularly the *RR*s. Taking into consideration the recent policies adopted in various countries that push toward more *RR* integration into the grid, there is an acute need for resource adequacy assessment tools that can explicitly account for the *RR* intermittent and stochastic nature. Consequently, in order to explicitly represent the time-varying nature and temporal correlations of system load and supply/demand resources, we veer from the random-variable-based

time-abstracted scheme to a random-process-based framework for resource adequacy assessment.

The time-dependent framework is a simulation-based construct for which assumptions $A\,1 - A\,3$ also hold. In the framework, we require the specification of the smallest indecomposable unit of time and of the study period for which we wish to perform resource adequacy assessment studies. Throughout this report we assume the smallest indecomposable unit of time to be one hour for a study period $\mathscr{T}_h$ consisting of H hours.

For the study period $\mathscr{T}_h$, we represent the system load as a discrete-time random process (*r.p.*) denoted by $\left\{\underset{\sim}{L}[h] \;:\; h = 1, 2, \ldots, H\right\}$. The *r.p.* is a collection of time-indexed *r.v.*s where each $\underset{\sim}{L}[h]$ represents the *r.v.* of the system load in hour h. The complete representation of the load by a *r.p.* further requires the specification of its sample space as well as of the probability law that maps each element of the sample space to the interval $[0, 1]$. The procedure of how to construct the sample space of the load *r.p.* has been extensively discussed in [18] and we adopt the same representation in this report. In effect, the sample space $\Omega_{\left\{\underset{\sim}{L}[h] \;:\; h=1,2,\ldots,H\right\}}$ of the system load *r.p.* is assembled by using historical data where each set of H hourly loads represents a sample path (*s.p.*) of $\left\{\underset{\sim}{L}[h] \;:\; h = 1, 2, \ldots, H\right\}$. Such a representation explicitly considers the time-correlations among hourly loads, since every historical *s.p.* has the time-correlation of the hourly loads embedded in it. Each *s.p.* is assumed to be equiprobable with probability one over the total number of *s.p.*s making up the sample space. An example of a *s.p.* for the load *r.p.* is shown in Fig. 2.2 for a week-long period.

For each conventional generation unit $g_k \in \mathscr{G}$, we denote by $\underset{\sim}{A}_k[h]$ the unit's available capacity *r.v.* in hour h. We further assume that, for each hour h the state of unit k is independent of the state of any other unit k', $k' \neq k$. Hence, $\underset{\sim}{A}_k[h]$ and $\underset{\sim}{A}_{k'}[h]$ are statistically independent *r.v.*s. In order to capture the variation of the availability of each conventional unit, we deploy a discrete Markov process with the appropriate number of states, where the transition times between states are assumed statistically independent and exponentially distributed *r.v.*s. As a side note, we clarify that it is necessary to "discretize" the continuous transition time *r.v.*s, in order to provide a consistent representation of both the system demand and unit availabilities in terms of the time resolution of the study period $\mathscr{T}_h$. A procedure of how to

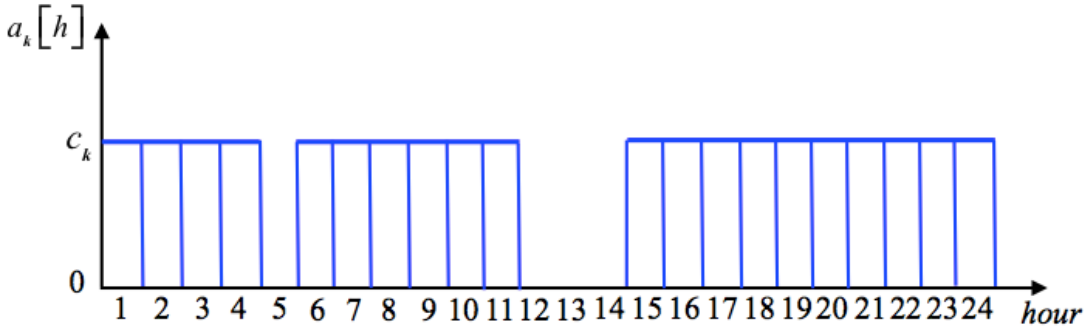

Figure 2.4: A day-long sample path for a two-state generation unit.

convert the continuous-time availability *s.p.*s to ones of hourly resolution is discussed in [18]. Therefore, we denote the availability of each unit $g_k \in \mathscr{G}$ by the discrete-time *r.p.* $\left\{ \underset{\sim}{A}_k[h] : h = 1, 2, \ldots, H \right\}$. By sampling the transition-time exponential distribution, we can determine the time period that the unit g_k spends at each of the capacity states. The statistical independence assumption allows for the construction of individual *s.p.*s for each $g_k \in \mathscr{G}$. The collection of hourly realizations $\{a_k[h] : h = 1, 2, \ldots, H\}$ constitutes a *s.p.* of resource g_k's available capacity and it essentially represents a sequence of states through which the unit passes over each hour of the period $\mathscr{T}_h$. We illustrate the concept of a *s.p.* for conventional generation resources with a simple example. Assume unit $g_k \in \mathscr{G}$ is described by only two states: the state *up* represents the state where the unit operates at full capacity c_k and the state *down* where the unit provides zero capacity. A sample path for the availability *r.p.* is an alternating sequence of periods that the unit spends in states *up* and *down* and is illustrated in Fig. 2.4. The methodology for simulating the available capacity of conventional generation resources is well documented in the literature and interested readers can refer to [19] for more details. We represent the total available capacity in the system by the discrete-time *r.p.* $\left\{ \underset{\sim}{A}_T[h] : h = 1, 2, \ldots, H \right\}$. From the *s.p.*s of the available capacity of each unit, we can derive the *s.p.* $\{a_T[1], a_T[2], \ldots, a_T[H]\}$ for the total available capacity where

$$a_T[h] = \sum_{k=1}^{G} a_k[h] \ , \tag{2.16}$$

for every $h \in \mathscr{T}_h$.

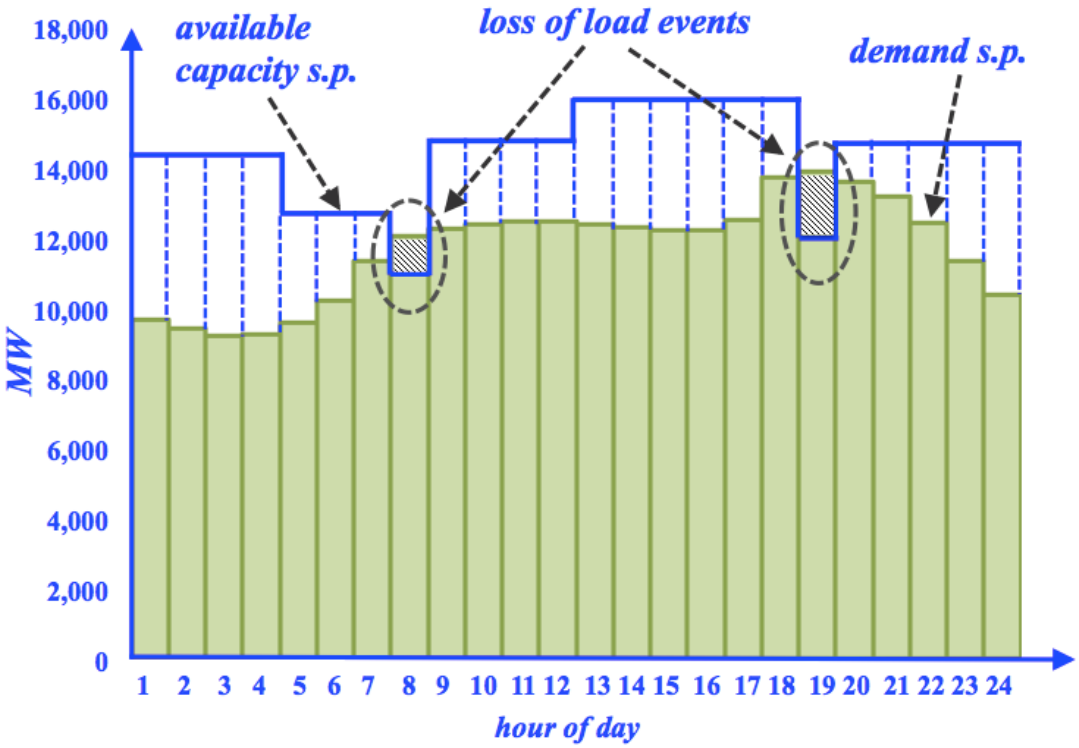

Figure 2.5: Determination of loss of load events via comparison of the demand and availability *s.p.*s.

The time-dependent framework makes use of the systematic sampling of the load and generation units availability *r.p.*s to simulate the behavior of the system and to generate the realizations of the loads and supply/demand resources. From the obtained realizations we can approximate the resource adequacy metrics of the sytem for the entire study period. More specifically, multiple runs of the simulation procedure are performed for a given study period $\mathscr{T}_h$. At every simulation run, *s.p.*s of the system load and generation unit availability are randomly sampled. The *s.p.*s of the units are combined to produce the *s.p.* of the total available capacity in the system. The realization of the load is superimposed on the realization of the total available capacity as illustrated in Fig. 2.5. By observing the realized behavior of the system, we count the $\ell.o.\ell.$ event occurrences and record their duration for the entire study period $\mathscr{T}_h$. From Fig. 2.5, we observe that two $\ell.o.\ell.$ events occurred during the day: one at 8 AM and the other at 7 PM, each of hourly duration. The example in Fig. 2.5 represents a single simulation run of the system, for a day study period. In order to produce estimates of the resource adequacy metrics with good fidelity, we need to repeat the experiment multiple times.

Issues regarding the number of simulation runs and the stopping criteria for the simulation procedure are discussed in [19].

We denote the total number of simulation runs by N and each run by i. Then, for each hour h and simulation run i we define the $\ell.o.\ell.$ event index

$$\beta^{(i)}[h] = \begin{cases} 1, & if\ \ell^{(i)}[h] - a_{T}^{(i)}[h] > 0 \\ \\ 0, & otherwise \end{cases} , \tag{2.17}$$

where $\ell^{(i)}[h]$ and $a_{T}^{(i)}[h]$ denote the realizations of $\underset{\sim}{L}[h]$ and $\underset{\sim}{A}_{T}[h]$ respectively at the i^{th} run. We further define the capacity deficiency for each hour h as $\delta^{(i)}[h] = \max\left\{0, \ell^{(i)}[h] - a^{(i)}[h]\right\}$. At the completion of simulation run i, the output $s.p.$s $\left\{\beta^{(i)}[h] : h = 1, 2, \ldots, H\right\}$ and $\left\{\delta^{(i)}[h] : h = 1, 2, \ldots, H\right\}$ for the $\ell.o.\ell.$ event index and the capacity deficiency are collected. Then, all the metrics of interest can be derived from the generated $s.p.$s. For example, the $LOLP$ for the computed period $\mathscr{T}_h$ is given by

$$\rho_{\mathscr{T}_h}^{(i)} = \sum_{h=1}^{H} \beta^{(i)}[h]\ \frac{hours}{H\ hours}\ . \tag{2.18}$$

The EUE can be evaluated as

$$u_{\mathscr{T}_h}^{(i)} = H \cdot \sum_{h=1}^{H} \delta^{(i)}[h]\ MWh\ . \tag{2.19}$$

To evaluate the $LOLE$ metric for the simulation run i, we require the knowledge of how many days in the study period experienced a $\ell.o.\ell.$ event. We can derive the $LOLE$ by the following procedure:

1. Since the study period $\mathscr{T}_h$ can be of any length H, we need to determine how many days are in $\mathscr{T}_h$. Therefore, we decompose $\mathscr{T}_h$ into $[D]$ non-overlapping subperiods, where $D = H/24$ and $[D]$ denotes the largest integer contained in D.

2. For each day $d = 1, 2, \ldots, [D]$, the subperiod

$$\mathscr{T}_h \big|_{\,d} = \{24(d-1) + h : h = 1, 2, \ldots, 24\}\ , \tag{2.20}$$

essentially represents the hours in day d.

3. We define the binary-valued index $\alpha^{(i)}[d]$ that takes value 1 if there exists at least one non-zero value of $\beta^{(i)}[h]$ in the set

$$\left\{\beta^{(i)}[24(d-1)+h] : h = 1, 2, \ldots, 24\right\} \ . \tag{2.21}$$

   Otherwise, $\alpha^{(i)}[d]$ takes the value zero.

4. We increase the index $d = d + 1$ and proceed to the next subperiod $\mathscr{T}_h \big|_d$.

5. When $d > [D]$, $\xi^{(i)}_{\mathscr{T}_h}$ is

$$\xi^{(i)}_{\mathscr{T}_h} = \sum_{d=1}^{[D]} \alpha^{(i)}[d] \ \frac{days}{D \ days} \ . \tag{2.22}$$

The final values of the metrics of interest, after N runs of the simulation procedure, can be approximated as the simple average of the generated sequence of N values. For example, the $LOLP$ index for the study period $\mathscr{T}_h$ is given by

$$\rho_{\mathscr{T}_h} \approx \frac{\sum_{i=1}^{N} \eta^{(i)}_{\mathscr{T}_h}}{N} \ . \tag{2.23}$$

Similarly, for the EUE

$$u_{\mathscr{T}_h} \approx \frac{\sum_{i=1}^{N} u^{(i)}_{\mathscr{T}_h}}{N} \ . \tag{2.24}$$

2.5 Conclusions

In this chapter we discussed two resource adequacy evaluation frameworks: the time-abstracted and time-dependent framework. We defined and provided the analytical expressions of the industry-wide resource adequacy metrics and discussed the mechanisms for the metrics consistent evaluation. The underlying assumption of the time resolution in the load model is key to understand the nature and meaning of each metric. However, the limitations of the time-abstracted framework in the representation of the uncer-

tain and time-varying nature of load and supply/demand resources motivated the development of a simulation-based scheme where load and resources are modeled as *r.p.*s, whose distribution has no analytical characterization. A salient aspect of the *r.p.* representation is the explicit consideration of the spatial and chronological correlations among the *s.p.*s of the loads and supply/demand resources. The systematic sampling of the *r.p.*s generates the realizations of the outputs of the loads and resources from which the resource adequacy metrics are evaluated for each simulation run. In Chapter 3 we describe how we make use of the time-dependent framework to explicitly represent the stochastic and intermittent nature of *RR*s and discuss the impacts of the deepening *RR* penetrations in the resource adequacy metrics.

CHAPTER 3

RESOURCE ADEQUACY ANALYSIS FOR SYSTEMS WITH INTEGRATED *RR*S

In this chapter, we make detailed use of the time-dependent framework to develop the approach for the assessment of resource adequacy for systems with integrated *RR*s. As a first step, we introduce the net load concept for the incorporation of *RR*s in the framework. Basically, we think of net load as the net difference between the total system load and the total *RR* outputs, in other words as the load that has to be met by the conventional resources. Clearly the net load, just as the *RR*s and the load, is itself a *r.p.* that effectively captures the intermittent and time-varying nature in the *RR* outputs. The framework with incorporated *RR*s is a sufficiently broad and comprehensive scheme that allows for the effective quantification of resource adequacy via the evaluation of the *LOLP*, *LOLE*, *LOLH* and *EUE* metrics. Our interests also lie in the investigation of the marginal behavior of the resource adequacy metrics with respect to the deepening *RR* penetrations. As such, we define and evaluate a set of sensitivity indices that aim to quantify the impacts of *RR* integration on the metrics of interest. The time-dependent framework with incorporated *RR*s is applicable to resource adequacy studies over short and longer-time periods and its implementation allows for the metrics evaluation even for data with different time resolutions.

3.1 The net load concept

The integration of large-scale *RR* generation into the grids introduces major challenges in the power system operation and planning regimes. Contrary to the conventional resources, *RR*s are non-controllable units due to their intermittent, stochastic and time-varying nature. The uncertain and intermittent nature of such resources is associated with fluctuating weather conditions, which are difficult to forecast accurately, particularly with long lead times.

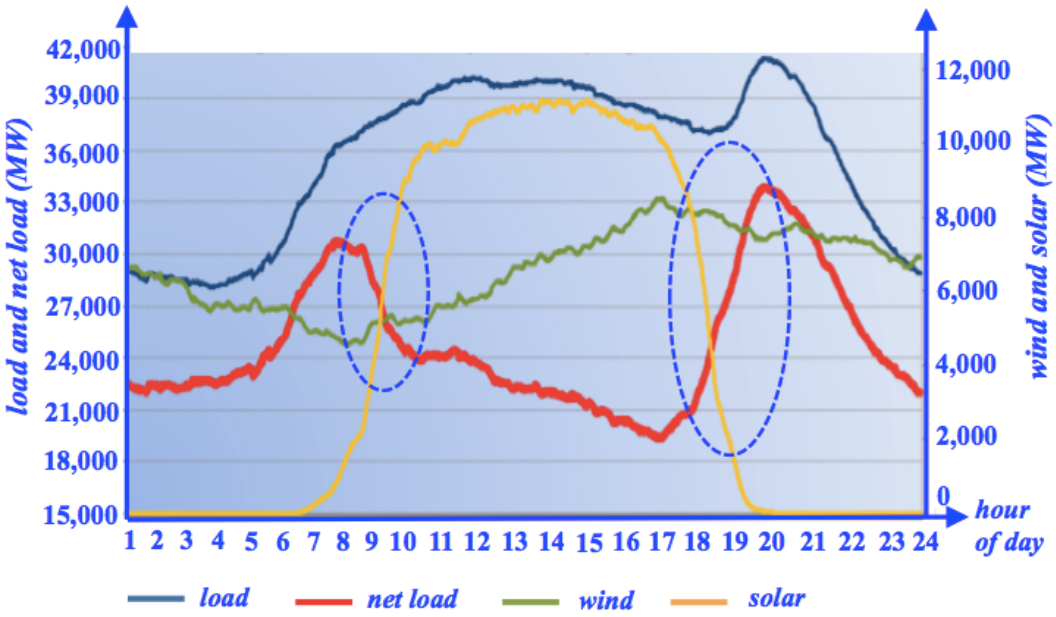

Figure 3.1: Projected load, net load and *RR* generation in *CAISO* for April 2020. (*Source: www.caiso.com*)

For example, the wind power output depends on the wind speed, whose predictability is problematic. As such, the *RR* expected power output is difficult to predict — in fact, it is generally more difficult to predict the *RR* power output than the system load [20]. The high variability in the *RR* outputs results in the reduced capability of such resources to track the system load. As illustrated in Fig. 3.1, during the course of the day, may occur multiple misalignments of the aggregate wind power generation with the system load. For example, between 5-9 AM and 6-8 PM, the load increases rapidly while the wind power output decreases. Solar generation appears to track more effectively the system load during the morning and mid-day hours, although it rapidly declines after 6 PM while the load is still high. Furthermore, the diagram reveals the requirements imposed to the conventional resources for tracking the net load, i.e., the net difference between the total system load and the total *RR* power outputs (including the net scheduled interchanges) [18]. From 6 to 7 PM, the net load change triples its magnitude while the *RR* generation declines, resulting in significant requirements for available generation capacity and ramping capability from conventional resources. Moreover, between 8-10 AM, the net load and the system load move in opposite directions. Consequently, the net load may be characterized by periods of steep

ramp-ups and down-ramps and may not exhibit the diurnal regularity pattern of the aggregate system load. However, the net load, by definition, incorporates the intermittent and time-varying effect of *RR*s. In the context of the time-dependent framework, we take advantage of the net load to extend the framework to take into consideration the *RR* stochastic and time-varying nature. In this regard, we represent the *RR*s as discrete-time *r.p.*s, similar to those of load and conventional supply resource representations. As such, the net load is also a discrete-time *r.p.*, whose *s.p.*s are constructed from the *s.p.*s of the *RR* and load *r.p.*s as detailed in the following section.

3.2 The time-dependent framework with incorporated *RR*s

We consider the system with G conventional resources and integrated groups of *RR*s from different technology types. We define a technology type group of *RR*s to be the set of all the integrated generation plants of the same renewable generation technology. For example, the set of all solar farms integrated into the grid constitutes a distinct *RR* technology type group. Similarly, the set of all the integrated wind farms constitutes another group. We assume there are Q technology type groups of *RR*s integrated into the system denoted by the set $\mathscr{Q} = \{q^k : k = 1, 2, \ldots, Q\}$, where each $q^k \in \mathscr{Q}$ corresponds to a group of *RR*s. For each group q^k, we denote the aggregate generation output of the group by the *r.p.* $\left\{\underset{\sim}{R}^k[h] : h = 1, 2, \ldots, H\right\}$. In order to construct a *s.p.* for $\underset{\sim}{R}^k[h]$, we make use of historical data[1] from multiple units in the group q^k. We represent the *RR* units that belong to group q^k by the set $\mathscr{W}^k = \{w_n^k : n = 1, 2, \ldots, W^k\}$ and the installed capacity of each unit in the set is denoted by κ_n^k. The set $\{r^k[h] : h = 1, 2, \ldots, H\}$ represents a *s.p.* for $\underset{\sim}{R}^k[h]$ such that

$$r^k[h] = \frac{\sum_{n=1}^{W^k} r_n^k[h]\kappa_n^k}{\sum_{n=1}^{W^k} \kappa_n^k}, \tag{3.1}$$

[1]We assume that the historical data for the construction of the sample space of *RR* *r.p.*s correspond to the same time period as the load historical data. Such practice aims to ensure that the weather correlation between demand and *RR* generation output is taken into consideration.

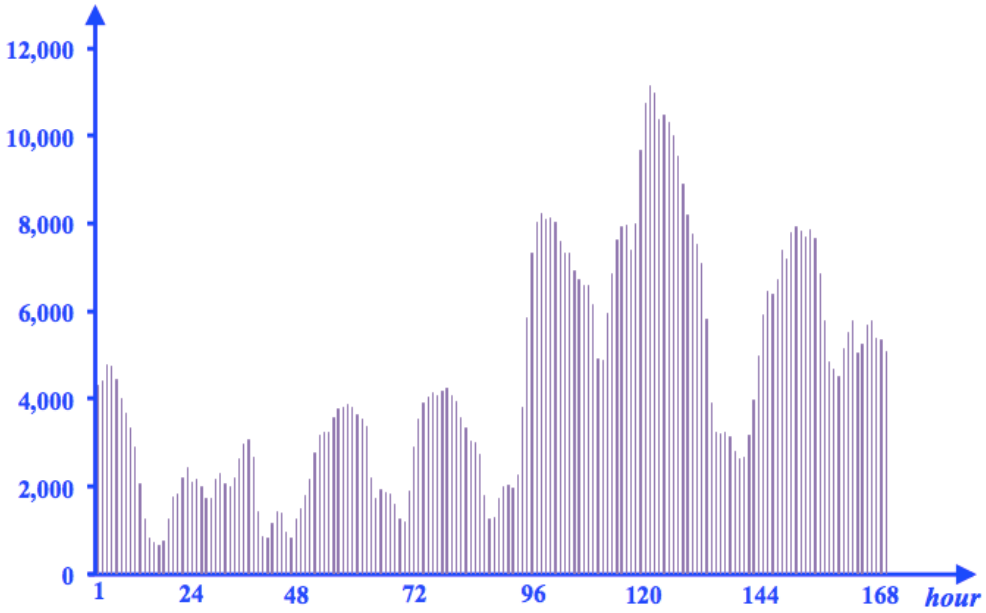

Figure 3.2: Chronological hourly *MISO* wind power output for the November 2-8, 2016 period. (*Source:www.misoenergy.org*)

where $r_n^k[h]$ denotes the generation output of RR unit n, in the technology type group q^k for hour h, obtained from historical data. Note that $r^k[h]$ represents the aggregate power output of all the RR units in the technology type group q^k. An example of a week-long *s.p.* for $\underset{\sim}{R}^k[h]$, with q^k representing the class of wind generation resources, is illustrated in Fig. 3.2.

For all the Q groups of RRs integrated into the grid, we define their aggregate generation output by the *r.p.* $\left\{\underset{\sim}{R}[h] : h = 1, 2, \ldots, H\right\}$ with *s.p.* $\{r[h] : h = 1, 2, \ldots, H\}$, derived from the *s.p.*s of $\underset{\sim}{R}^k[h]$ as follows

$$r[h] = \sum_{k=1}^{Q} r^k[h] \ . \tag{3.2}$$

For a study period $\mathscr{T}_h$ and at a specified level of installed RR capacity κ^k, we define the generation penetration of the RR group q^k as the ratio of the total generation from RRs in the group over the total energy produced by all the system supply resources in the period. We denote the generation penetration of the RR group q^k by γ^k. We emphasize that each γ^k is a function of the installed RR capacity κ^k, the system loads and supply/demand resource generation. As such, the values of γ^k are obtained after the realizations of

the system load, conventional resource availability and RR generation output $r.p.$s. We define the vector of RR installed capacity $\underline{\boldsymbol{\kappa}} \in \mathbb{R}^Q$ as

$$\underline{\boldsymbol{\kappa}} = \left[\kappa^1 \ \kappa^2 \ \ldots \kappa^Q\right]^\dagger, \tag{3.3}$$

and the RR penetration vector

$$\underline{\boldsymbol{\gamma}} = \left[\gamma^1 \ \gamma^2 \ \ldots \gamma^Q\right]^\dagger, \tag{3.4}$$

with entries the penetrations of each group of RRs. At a specified level of RR installed capacity $\underline{\boldsymbol{\kappa}}$, we incorporate the RRs in the resource adequacy framework via the system load modification: we subtract each aggregate RR generation output $s.p.$ from the system load $s.p.$ that corresponds to the same time-period. The generated $s.p.$ represents a $s.p.$ for the net load. In mathematical terms, we represent the net load at a level of $\underline{\boldsymbol{\kappa}}$ RR installed capacity, by the discrete-time $r.p.$

$$\left\{ \underset{\sim}{L}[h]\Big|_{\underline{\boldsymbol{\kappa}}} = \underset{\sim}{L}[h] - \underset{\sim}{R}[h] : h = 1, 2, \ldots, H \right\}, \tag{3.5}$$

with a $s.p.$ given by the set

$$\left\{ \ell[h]\Big|_{\underline{\boldsymbol{\kappa}}} = \ell[h] - r[h] : h = 1, 2, \ldots, H \right\} . \tag{3.6}$$

Each $s.p.$ has an associated probability equal to one over the total number of $s.p.$s in the sample space of $\underset{\sim}{L}[h]\Big|_{\underline{\boldsymbol{\kappa}}}$. The computational procedure for the evaluation of the $LOLP$ and all the other resource adequacy metrics remains unchanged in the time-dependent scheme for the realizations of the net load, at the specified level of RR installed capacity $\underline{\boldsymbol{\kappa}}$. Fig. 3.3 shows a single-day net load $s.p.$ that is compared with the daily $s.p.$ of the total available capacity. For the particular realization of the system net load and supply availability, we can readily register the occurrence of the $\ell.o.\ell.$ events — namely the single event at 7 PM — and measure its magnitude. The time-dependent evaluation procedure with incorporated RRs, entails the collection of the total number of $\ell.o.\ell.$ event occurrences as well as their magnitude, for multiple and repeated realizations of the system net load and conventional resource availability. In effect, the computational procedure is exactly similar

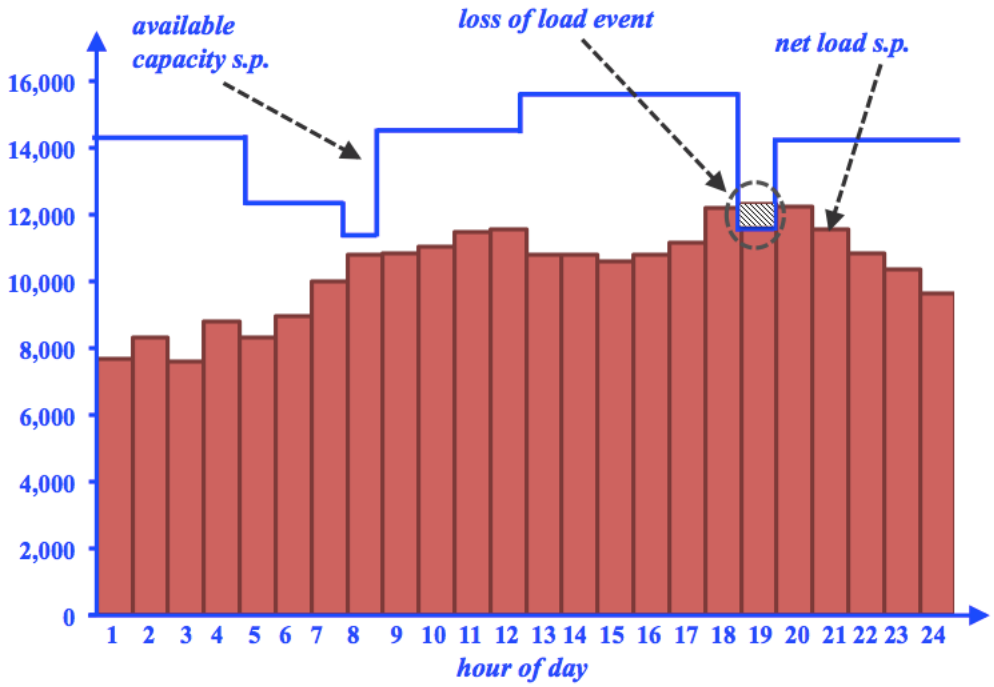

Figure 3.3: Determination of loss of load events via comparison of the net load and available capacity *s.p.*s.

with the case where *RR*s are not incorporated in the framework, i.e., $\underline{\boldsymbol{\kappa}} = \underline{\mathbf{0}}$. Therefore, we view the time-dependent framework with incorporated *RR*s as a generalized scheme that can be applied for any value of $\underline{\boldsymbol{\kappa}}$.

We define for each hour h and each simulation run i, the hourly $\ell.o.\ell.$ event index

$$\beta^{(i)}[h]\Big|_{\underline{\boldsymbol{\kappa}}} = \begin{cases} 1, & if\ \ell^{(i)}[h]\Big|_{\underline{\boldsymbol{\kappa}}} - a^{(i)}[h] > 0 \\ \\ 0, & otherwise \end{cases} . \tag{3.7}$$

We further define the capacity deficiency for each hour h as

$$\delta^{(i)}[h]\Big|_{\underline{\boldsymbol{\kappa}}} = \max\left\{0,\ \ell^{(i)}[h]\Big|_{\underline{\boldsymbol{\kappa}}} - a^{(i)}[h]\right\} . \tag{3.8}$$

The *LOLP* for the entire period $\mathscr{T}_h$ is given by

$$\rho^{(i)}_{\mathscr{T}_h}\Big|_{\underline{\boldsymbol{\kappa}}} = \sum_{h=1}^{H} \beta^{(i)}[h]\Big|_{\underline{\boldsymbol{\kappa}}} \frac{hours}{H\ hours} . \tag{3.9}$$

Similarly, the *EUE* can be evaluated by

$$u^{(i)}_{\mathscr{T}_h}\Big|_{\underline{\boldsymbol{\kappa}}} = H \cdot \sum_{h=1}^{H} \delta^{(i)}[h]\Big|_{\underline{\boldsymbol{\kappa}}} \; MWh \; . \tag{3.10}$$

The computation of the *LOLE* requires the evaluation of the daily $\ell.o.\ell.$ event index

$$\alpha^{(i)}[d]\Big|_{\underline{\boldsymbol{\kappa}}} = \begin{cases} 1, & if \;\; \beta^{(i)}[h]\Big|_{\underline{\boldsymbol{\kappa}}} > 0, \;\; \forall h \in \mathscr{T}_h \,\big|_{\,d} \\ \\ 0, & otherwise \end{cases} \; . \tag{3.11}$$

Then, the *LOLE* for the period $\mathscr{T}_h$ can be derived as

$$\xi^{(i)}_{\mathscr{T}_h}\Big|_{\underline{\boldsymbol{\kappa}}} = \sum_{d=1}^{[D]} \alpha^{(i)}[d]\Big|_{\underline{\boldsymbol{\kappa}}} \; \frac{days}{D \;\; days} \; . \tag{3.12}$$

After N simulation runs, the final values of all resource adequacy metrics are assessed as the simple average of the sequence of N values, each value generated at the end of every simulation run. For example, the *LOLE*

$$\xi_{\mathscr{T}_h}\Big|_{\underline{\boldsymbol{\kappa}}} \approx \frac{\sum_{i=1}^{N} \xi^{(i)}_{\mathscr{T}_h}\Big|_{\underline{\boldsymbol{\kappa}}}}{N} \; . \tag{3.13}$$

3.3 Impacts of integrated *RR* capacity additions

In Section 3.2 we developed the framework to evaluate the resource adequacy metrics for systems with integrated *RR* capacity. We are particularly interested to provide a quantification of the impacts of *RR* integration on the resource adequacy metrics. In this regard, we augment the set of metrics with new sensitivity indices with the objective to measure each metric's sensitivity with respect to the penetration $\gamma^{\,k}$ around a reference penetration level $\underline{\boldsymbol{\gamma}}_0$. More specifically, if we assume a small variation $\delta\gamma^{\,k}$ for the *RR* group $q^{\,k}$, then the sensitivity of the resource adequacy metric χ with respect

to $\gamma^{\,k}$ is defined as

$$\psi^{\chi}_{\gamma^{\,k}}\Big|_{\underline{\boldsymbol{\gamma}}_0} = \frac{\chi\big|_{\underline{\boldsymbol{\gamma}}_0+\underline{\mathbf{1}}^{\,k}\delta\gamma^{\,k}} - \chi\big|_{\underline{\boldsymbol{\gamma}}_0}}{\delta\gamma^{\,k}}, \tag{3.14}$$

where $\underline{\mathbf{1}}^{\,k} = [0, 0, \ldots, 1, \ldots, 0]^T$ with entry 1 in the k^{th} row. The sensitivity index $\psi^{\chi}_{\gamma^{\,k}}\Big|_{\underline{\boldsymbol{\gamma}}_0}$ captures the change in the resource adequacy metric χ with respect to $\gamma^{\,k}$ and aims to provide additional insights on how each group of RRs may have different influence on the resource adequacy of the system.

To understand how the integration of RRs impacts the resource adequacy of the system, we look on the representation of such resources in the time-dependent framework. In effect, the incorporation of RRs is embedded in the net load, which implies that the conventional generation resources of the system with $\underline{\boldsymbol{\kappa}} \neq \underline{\mathbf{0}}$, must meet, each hour, a load value that is less than or equal to the load faced when $\underline{\boldsymbol{\kappa}} = \underline{\mathbf{0}}$. The fact that the output of a RR is a non-negative quantity implies that there is a non-negative contribution to the system resource adequacy associated with the integration of a non-zero RR capacity. Therefore we can write

$$\rho_{\mathscr{T}_h}\Big|_{\underline{\boldsymbol{\kappa}}} \leq \rho_{\mathscr{T}_h}\ . \tag{3.15}$$

The main idea behind inequality (3.15) can be readily captured in the context of the time-dependent framework if we think that in every simulation run the realization of the conventional capacity availability is compared with the realization of the net load, whose hourly *s.p.* values are in the worst case equal to the load *s.p.* for $\underline{\boldsymbol{\kappa}} = \underline{\mathbf{0}}$. Consequently, the sum of the elements in the set $\left\{\beta^{(i)}[h]\Big|_{\underline{\boldsymbol{\kappa}}} : h = 1, 2, \ldots, H\right\}$ is bounded above by the sum of the elements in $\left\{\beta^{(i)}[h] : h = 1, 2, \ldots, H\right\}$. We can further verify such physically intuitive outcomes through the deployment of the analytical means offered by the time-abstracted framework. Recall that the $LOLP$ is evaluated as the sum of the cumulative probabilities $\phi(\ell_h)$ at a specified load level ℓ_h. However, cumulative probabilities satisfy the non-decreasing property: if $\ell_h \leq \ell_{h'}$ then $\phi(\ell_h) \leq \phi(\ell_{h'})$. Given that the $LOLP$ is simply the sum of the non-negative quantities $\phi(\cdot)$ over the specified period $\mathscr{T}_h$, we can deduce that the $LOLP$ for a system with $\underline{\boldsymbol{\kappa}} \neq \underline{\mathbf{0}}$ is bounded above by the $LOLP$ for the system with $\underline{\boldsymbol{\kappa}} = \underline{\mathbf{0}}$. Given that $\phi(\cdot)$ is the building block for the $LOLH$, $LOLE$ and EUE, we can derive analogous inequalities to (3.15) for all the resource adequacy

metrics. We emphasize that inequality (3.15) holds under the assumption that the set of conventional generation resources does not change throughout the study period $\mathscr{T}_h$. In other words, no conventional generation capacity is retired or displaced by RRs at any hour $h \in \mathscr{T}_h$. Therefore, the integration of RR generation capacity to the fleet of conventional resources, can only have a non-negative impact on the resource adequacy within the time-dependent framework.

3.4 Conclusions

In this chapter we discussed the net load concept and its salient characteristic: the ability to effectively incorporate the intermittent and time-varying nature of RRs. We take advantage of the net load to generalize the time-dependent framework so as to take into account any RR technology type group. By making use of historical RR output data we construct the $s.p.$s of the RR $r.p.$s, which we subtract from the load $s.p.$s to derive the $s.p.$s of the net load. The time-dependent resource adequacy evaluation framework is similar for the net load representation to the framework discussed in Chapter 2. In order to investigate the impacts of deepening RR penetrations in the resource adequacy, we augment the set of resource adequacy metrics with sensitivity indices that measure the sensitivity of each primary metric with respect to the deepening penetrations of each RR group. The non-negative output of RRs, leads to the conclusion that RR capacity has a non-negative contribution in the resource adequacy. As such, the values of the resource adequacy metrics for the system with integrated RR capacity are bounded above by the values of the metrics for the system with zero RR capacity — provided that the set of conventional resources does not change. In Chapter 4 we present representative applications of the time-dependent framework with incorporated RRs and evaluate the augmented set of indices for two distinct cases: RRs are integrated into the existing fleet of conventional generation resources and, RRs are integrated by displacing conventional resources.

CHAPTER 4

NUMERICAL STUDY RESULTS

We devote this chapter to discuss a set of representative studies that we obtain with the application of the resource adequacy evaluation framework presented in Chapter 3. We are particularly interested in longer-term planning studies with a specific focus on the investigation of the impacts of deepening *RR* penetrations on the resource adequacy metrics. We capture the marginal behavior of each resource adequacy metric through a set of sensitivity indices in order to provide valuable insights in the way each group of *RR*s affects each metric in particular. Through extensive applications of the framework we study the coupled effects of the deepening *RR* penetrations with the retirement of conventional generation units. We analyze numerous cases of *RR* penetrations and conventional capacity replacements. The sensitivity studies carried out provide meaningful insights in the behavior of the resource adequacy metrics with respect to the factors of influence considered and highlight the limitations of *RR*s in the provision of resource adequacy.

4.1 The scope and nature of the studies

The focus of the application studies reported here is on solar and wind *RR*s. We apply the resource adequacy evaluation framework in a large-scale, representative test system.[1] The studies performed use scaled historical load data from the geographical footprint of the New York state control area (*NYCA*) from 2011 to 2015.[2] The annual summer peak load forecast for 2030 is equal $36,800$ MW. Forecasts until the year 2026 and projection methodologies for the *NYCA* are extensively provided in the annual "Gold Book" [21]. The

[1] The details of the test system are available online at: https://github.com/Mariola-Nd/master-thesis-data.

[2] Available online at: http://www.nyiso.com/public/markets_operations/market_data/load_data/index.jsp.

conventional generation resources in the system have a total nameplate capacity of $31,500$ MW and include coal, gas, oil and nuclear units. The system also incorporates $6,000$ MW of hydro renewable resources, which are modeled as a constant injection. The imports into the system are also represented as a constant injection of $2,500$ MW. We assume no *DRR*s in the system, i.e., all the demand is met by conventional generation units and *RR*s. Under this assumption, we, in effect, consider a worst-case condition and as such, the values of the resource adequacy metrics may be viewed as upper bounds, since any deployment of *DRR*s has the impact to improve each resource adequacy metric. We model each conventional generation resource as a two-state unit with its own *FOR*. The imports are modeled as a conventional generation unit that is 100 % available — in effect as a reduction of the load by $2,500$ MW. For the studies, we use *FOR* data from the *NERC* generation availability data system (*GADS*). For the representation of the wind and solar farms, we have 5-year historical wind and solar data from the geographical footprint of *NYCA* for the 2011-2015 period.[3] The 12 wind farms and the seven solar farms are spread at various locations in the *NYISO* footprint. The nameplate capacities of the integrated wind and solar generation resources are $15,000$ MW and $4,000$ MW, respectively.

To study the effects of the deepening *RR* penetrations on the resource adequacy metrics, we perform two sets of studies on the system. In the first study set, we consider the grid with the integrated solar and wind farms and the existing fleet of conventional resources. We evaluate the *LOLE*, *LOLH* and *EUE* metrics for each specified pair of solar and wind capacity values and compute their associated sensitivities as defined in (3.14). In the second study set we assess the impacts of the retirement of conventional generation capacity on the resource adequacy metrics. In the latter case, solar and wind resources are integrated into the grid via the gradual replacement of conventional capacity. Such an implementation provides a more realistic perspective on the effects of deepening *RR* penetrations into the grid's resource adequacy as the integration of *RR*s aims to replace polluting fossil-fired generation resources. The application and sensitivity studies are carried out for a period of 8760 hours for the year 2030.

[3]The solar data are available online at: https://github.com/Mariola-Nd/master-thesis-data. The wind generation data are available online at: https://github.com/mikerahk/FoDS_Capstone/tree/master/Data.

In the application studies, we construct 59 different cases of integrated solar and wind capacities that correspond to different generation penetrations, i.e., different values of $\underline{\boldsymbol{\gamma}} = [\gamma^s,\ \gamma^w]^\dagger$. From this point on, we use superscript s and w notation to denote the group of solar and wind resources respectively in order to facilitate our discussion of the study results. We define the set of cases $\mathscr{C} = \{c_j : j = 1, \ldots, 59\}$ where each case c_j is represented by the capacity vector $\underline{\boldsymbol{\kappa}}_j = \left[\kappa_j^s,\ \kappa_j^w\right]^\dagger$, which corresponds to the penetration vector $\underline{\boldsymbol{\gamma}}_j = \left[\gamma_j^s,\ \gamma_j^w\right]^\dagger$. Clearly, $\underline{\boldsymbol{\kappa}}_1 = [0,\ 0]^\dagger$ results in $\underline{\boldsymbol{\gamma}}_1 = [0,\ 0]^\dagger$, i.e., the system has zero generation penetrations of solar and wind resources in the case c_1. The study case c_{59} corresponds to $\underline{\boldsymbol{\kappa}}_{59} = [4,000,\ 15,000]^\dagger$ and gives $\underline{\boldsymbol{\gamma}}_{59} = [6.03\ 20.06]^\dagger$, i.e., the maximum total generation penetration of solar and wind obtained is 26.09%. The study system has a 25% penetration from renewable hydro generation and as such, to achieve the goal of 50% total penetration from *RR*s, we need an additional 25% from wind and solar resources. Therefore, the goal of 50% *RR* penetration is achieved for the study system in case c_{59}. Note that such a penetration level corresponds to the case where the fleet of conventional generation resources remains intact. The *RR* penetrations will change considerably once the retirement of conventional capacity is taken into account.

We construct the 59 cases by the combination of nine values for κ_j^s and 11 values for κ_j^w. For the solar capacity, κ_j^s, takes values from 0 MW to 4,000 MW with increments of 500 MW. The wind installed capacity, κ_j^w, takes values from 0 MW to 15,000 MW with increments of 1,250 MW. We do not consider every possible combination (9×11) of κ_j^s and κ_j^w, but rather limit the framework applications to a subset of combinations that are representative and sufficient to derive meaningful results. For each case, the system has a specific value of total installed solar and wind capacity denoted by κ_j^s and κ_j^w respectively.

To evaluate the metric sensitivities under the retirement of conventional capacity we introduce the notion of a retirement fraction denoted by ζ. We define the retirement fraction as the fraction of the retired conventional capacity of the total solar and wind capacity added. We carry out simulation studies with the retirement fraction ζ assuming the values in the set

$$\mathscr{Z} = \{\zeta_i = 0.05i, i = 1, 2, ..., 18\}\ . \tag{4.1}$$

For example, $\zeta_2 = 0.1$ implies that for 100 MW of nameplate solar and wind capacity integrated in the system, 10 MW of conventional capacity is retired. We construct a total of 373 cases from a subset of cases $c_j \in \mathscr{C}$ and for each $\zeta_i \in \mathscr{Z}$ and evaluate the resource adequacy metrics. Note that the resulting solar and wind penetrations in each case depend both on the values of the installed wind and solar capacities but also on the values of ζ_i.

4.2 The study results

We discuss the key results and findings for the first set of studies without the combination of retirements in the resource mix. We start out with the presentation of the values of the resource adequacy metrics — *LOLE*, *LOLH* and *EUE* — with respect to γ_j^s and γ_j^w. In Figs. 4.1 to 4.3 we plot each resource adequacy metric for a set of representative cases. The complete results for each case considered are listed in the Appendix C of this report. Each point in the diagrams represents a different case, which corresponds to a distinct pair of values $\left[\gamma_j^s, \gamma_j^w\right]^\dagger$. The horizontal axis represents the penetration of integrated solar capacities and each scattered line indicated by different symbol and color, corresponds to distinct wind generation penetrations. As we move horizontally in the diagram from left to right, the solar generation penetrations deepen while moving from the top to bottom vertically, the penetrations of wind generation deepen.

We note that the results indicate that each metric decreases as the penetrations of wind and/or solar generation increase. For example, the *LOLE* for case c_1 is equal to 0.06 days/year and it drops to approximately 0.01 days/year for scenario c_{59} ($[\gamma_{59}^s\ \gamma_{59}^w]^\dagger = [6.03,\ 20.06]^\dagger$). If the study system were to comply to the $LOLE \leq 0.1$ days/year criterion, then the system is resource adequate even in the case c_1. Thus the installed conventional generation resource capacity and the imports from neighboring entities suffice to meet the system's total forecasted load in 2030 without any integrated wind/solar resources.

Similar decline with the *LOLE* is observed on both the *LOLH* and *EUE* metrics. For example, the *LOLH* index drops from 0.182 hours/year to 0.025 hours/year for cases c_1 and c_{59} respectively. The corresponding values for the *EUE* are 273.0 MWh/year which drops to only 20.805 MWh/year. The

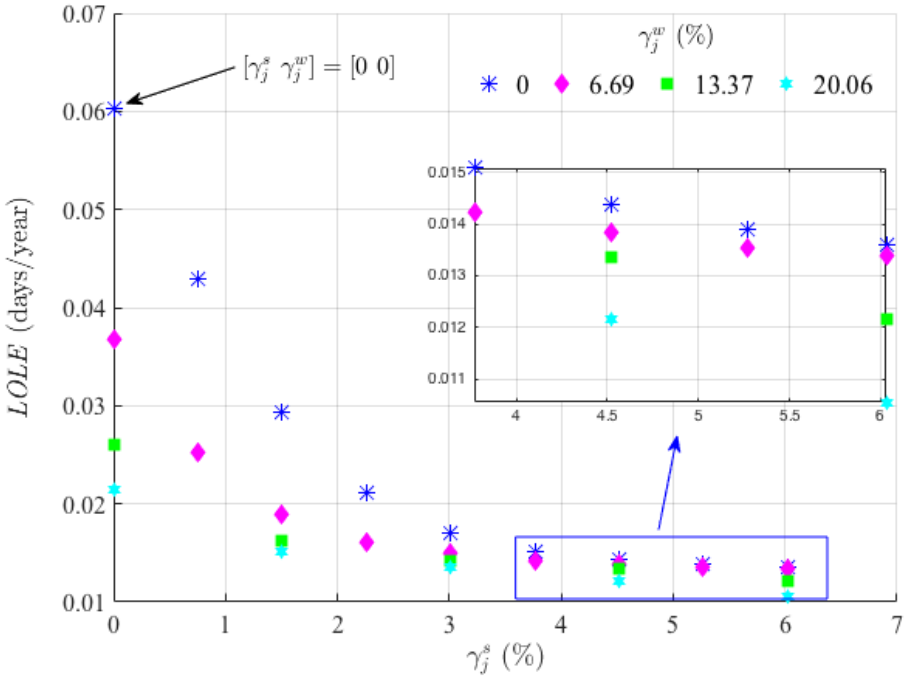

Figure 4.1: *LOLE* values for different wind and solar penetrations.

decline in the resource adequacy indices is certainly not surprising. It is

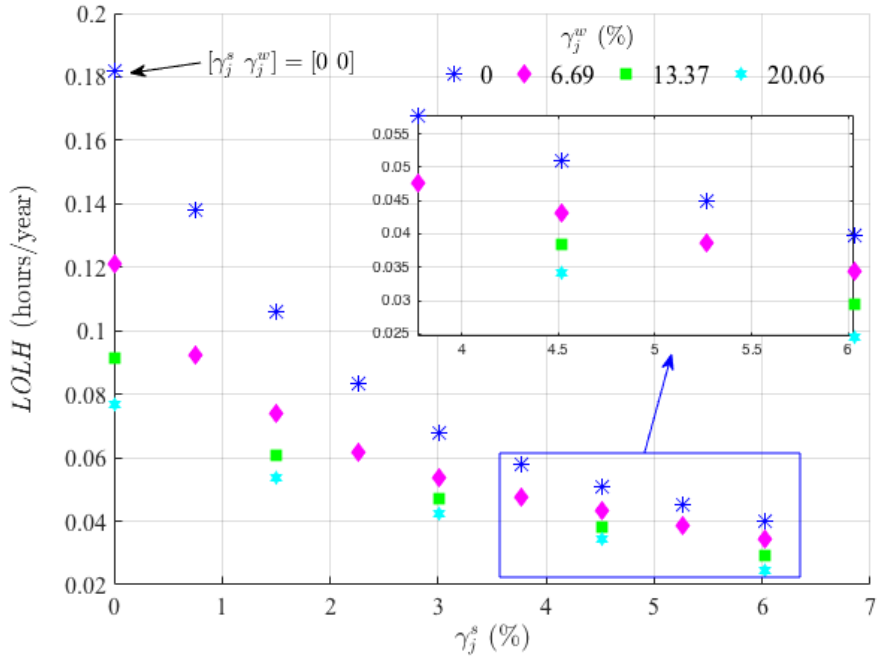

Figure 4.2: *LOLH* values for different wind and solar penetrations.

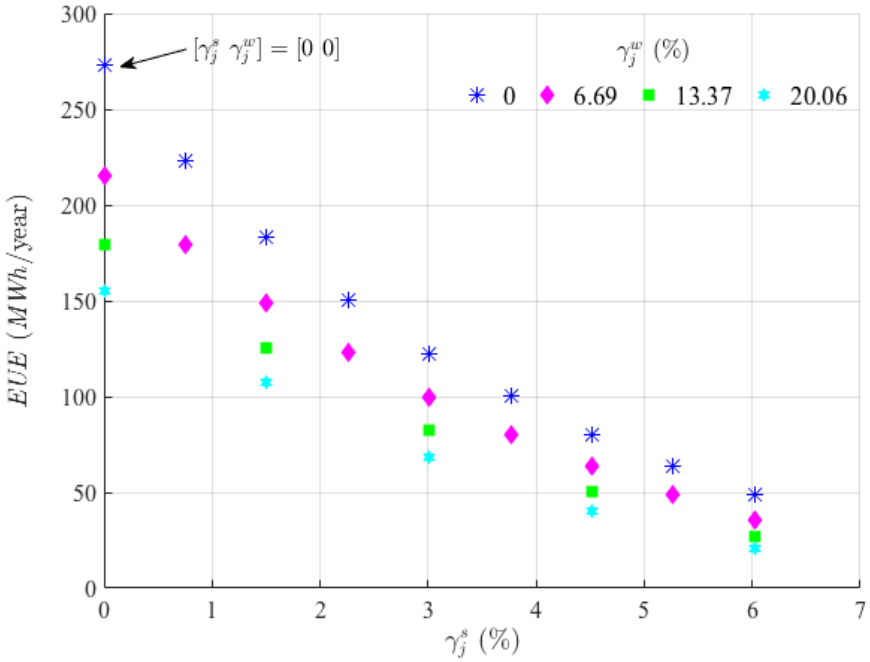

Figure 4.3: EUE values for different wind and solar penetrations.

worthwhile to note that a 6.69% penetration of wind generation alone, has a significant impact on the metrics. Under such conditions, which correspond to case c_5, with $[\gamma_5^s\ \gamma_5^w]^\dagger = [0,\ 6.69]^\dagger$, the $LOLE$ metric exhibits a drop of approximately 50%, from 0.06 to 0.0368 days/year. Similar impacts are observed on the $LOLH$ and EUE values. However, we note that the decline in the resource adequacy metrics is diminishing as the penetrations of wind and solar deepen. Indeed, the scatter "curves" become flatter (less sloped) as we move towards the right. The behavior of the metrics indicates diminishing marginal returns, which implies that the contribution of 1 MW of integrated solar and wind capacity to the improvement in resource adequacy is significantly smaller at $\underline{\boldsymbol{\gamma}}_{56} = [6.03,\ 10.04]^\dagger$ than at $\underline{\boldsymbol{\gamma}}_3 = [0,\ 3.35]^\dagger$. To verify the diminishing returns, we evaluate the sensitivities of each resource adequacy metric as defined in (3.14).

In Figs. 4.4 and 4.5 we present the absolute sensitivity values of the $LOLE$ with respect to the wind and solar generation penetrations, respectively. From these plots we observe that the sensitivity of the $LOLE$ decreases as the penetrations of wind and solar generation increase. The results indicate that the reduction in the $LOLE$ becomes smaller as we deepen the RR pen-

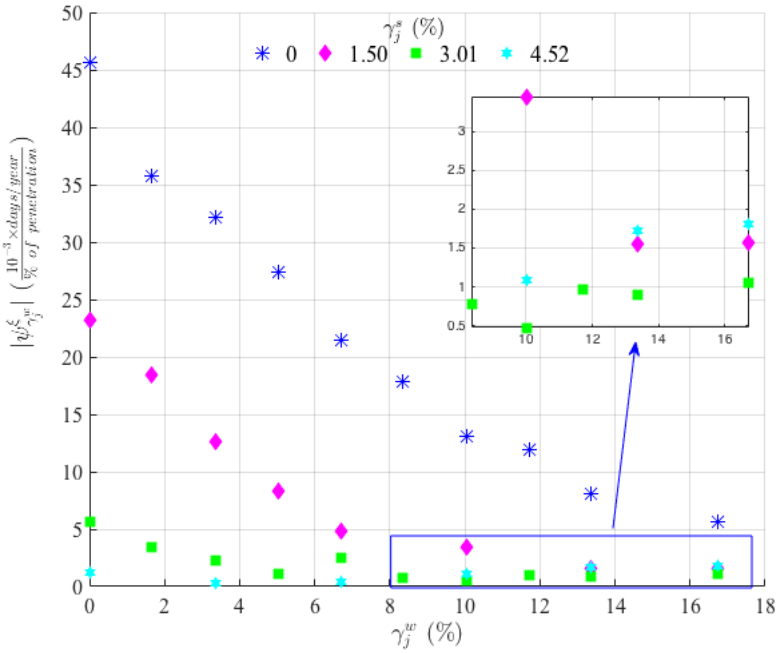

Figure 4.4: Sensitivity of the *LOLE* metric with respect to wind generation penetration.

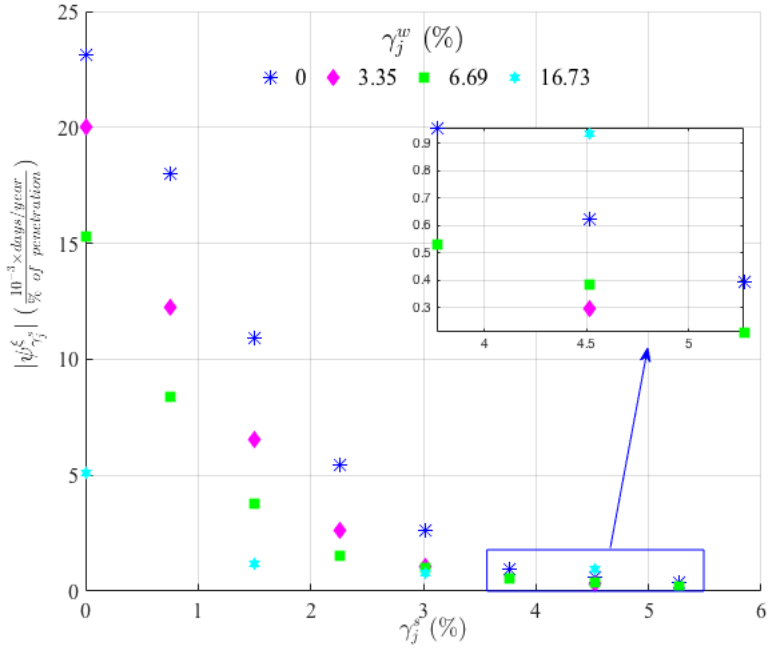

Figure 4.5: Sensitivity of the *LOLE* metric with respect to solar generation penetration.

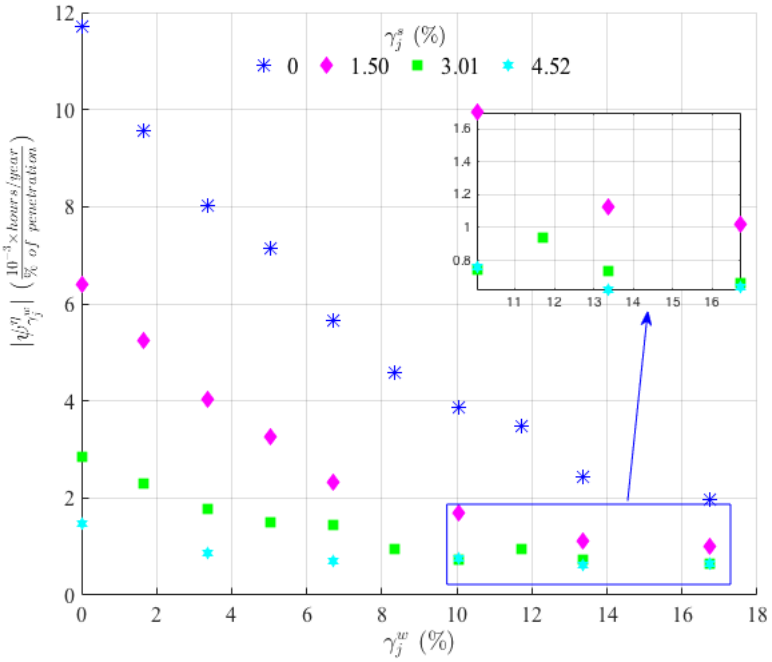

Figure 4.6: Sensitivity of the *LOLH* metric with respect to wind generation penetration.

etrations into the grid. For example, from Fig. 4.4 we note that for $\gamma_j^s = 0$, an increase of γ_1^w from 0 % to γ_2^w at 1.67 % results in a decrease of the *LOLE* of approximately 45.69×10^{-4} days/year/% of penetration. However, an increase of γ_9^w from 13.37 % to γ_{10}^w 16.73 % results in the reduction of the *LOLE* by only 8.05×10^{-4} days/year/% of penetration. Similar conclusions are drawn for the sensitivity of the *LOLE* index with respect to solar generation penetrations. Another interesting observation is that for only 4.52% solar penetration (cyan-colored stars), the decrease in the *LOLE* is slightly greater than zero for a change of wind penetration from 3.35% to as high as 16%. For this test system, the comparative sensitivities under deepening solar and wind penetrations are 10 times more impactful for each % change in solar penetration than in wind penetration. Although the deepest solar generation penetration is about a third of the deepest wind penetration in these application studies, solar appears to be a far more impactful choice than wind to improve the resource adequacy of the system.

We observe similar behavior in the sensitivities of the *LOLH* and *EUE* to changes in wind and solar penetrations. We provide some illustrative rep-

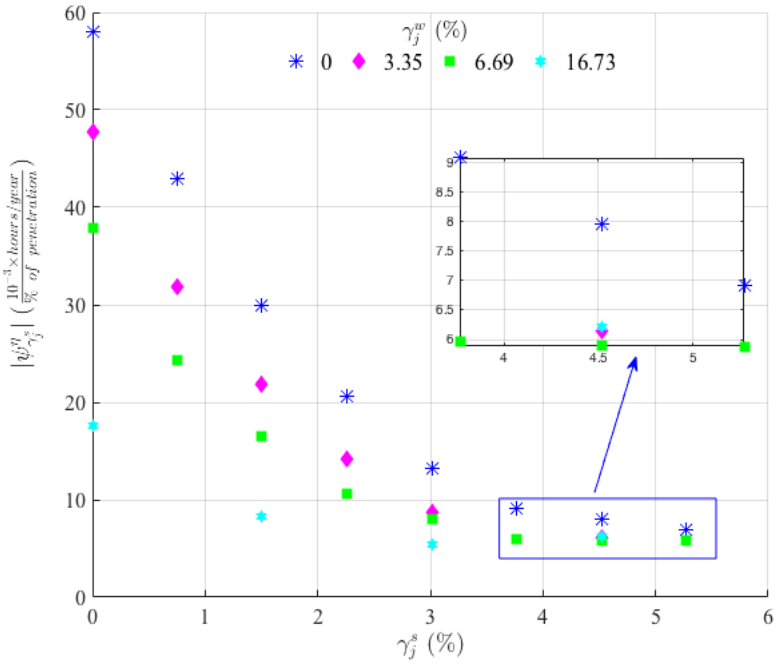

Figure 4.7: Sensitivity of the *LOLH* metric with respect to solar generation penetration.

resentative results in Figs. 4.6 – 4.9. We observe from the diagrams that a change in $\gamma_0^w = 0\%$ to $\gamma_1^w = 1.67\%$ results in the decrease of the *LOLH* by 12×10^{-3} hours/year/% of penetration. However, a change in $\gamma_0^s = 0\%$ to $\gamma_1^s = 0.75\%$ — less than half the increase in the wind penetration — drops the *LOLH* by 57.98×10^{-3} hours/year/% of penetration. The *EUE* metric exhibits a decrease by 10.67 MWh/year/% of penetration for a change in $\gamma_0^w = 0\%$ to $\gamma_1^w = 1.67\%$ and by 66.15 MWh/year/% of penetration for an increase in $\gamma_0^s = 0\%$ to $\gamma_1^s = 0.75\%$. However, a 0.75% percent change in γ_j^s for the cases $\gamma_7^s = 5.27\%$ to $\gamma_8^s = 6.03\%$ results in a decrease of the *LOLH* by only 6.92×10^{-3} hours/year/% of penetration. This result is significantly lower than the 57.98×10^{-3} hours/year/% of penetration obtained for an equivalent change in the γ_j^s and indicates the diminution of the marginal returns with deepening solar penetrations. Similar results are obtained for the *EUE* metric for deepening *RR* penetrations. Such outcomes in the metrics values indicate that the contribution of 1 MW of integrated solar/wind capacity to the resource adequacy of the system diminishes as the solar/wind penetrations deepen.

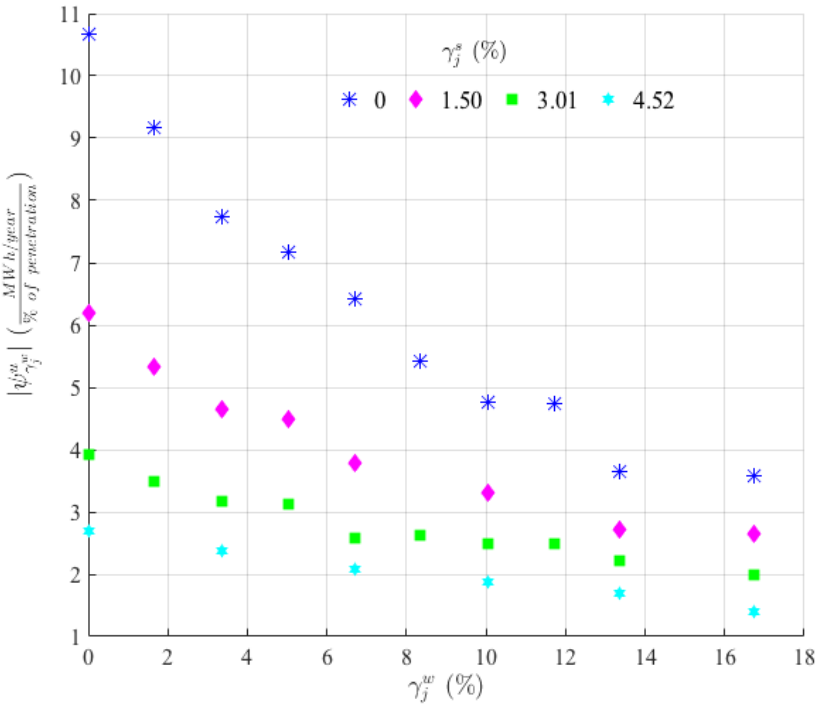

Figure 4.8: Sensitivity of the *EUE* metric with respect to wind generation penetration.

4.3 The retirement case

In the second set of the sensitivity studies we evaluate the resource adequacy metrics with respect to γ_j^s, γ_j^w and ζ_i. For each value of ζ_i we require that the system satisfies the "1 day in 10 years" resource adequacy criterion, i.e., *LOLE* less than or equal to 1 days in 10 years. Therefore, any combination of values of $\underline{\boldsymbol{\gamma}}_j$ and ζ_i that results in *LOLE* strictly greater than 1 day in 10 years, is assumed to make the system inadequate to supply its forecasted load in 2030. In Figs. from 4.10 to 4.14 we plot the *LOLE* metric for different values of ζ_i and *RR* penetrations. The abscissa (ordinate) in the diagrams represents solar (wind) generation penetrations. The center of each circle in the diagram corresponds to a distinct pair of $\left[\gamma_j^s, \gamma_j^w\right]^\dagger$ for a specified value of ζ_i. The size of each circle represents the value of the *LOLE* metric. Our focus is not at the exact value of the *LOLE* at each case but rather wish to investigate how the solar and wind penetrations affect the *LOLE* at a specified conventional resource retirement fraction. Each circle in Fig. 4.10 depicts the *LOLE* value that results under $\zeta_2 = 0.1$, i.e., for

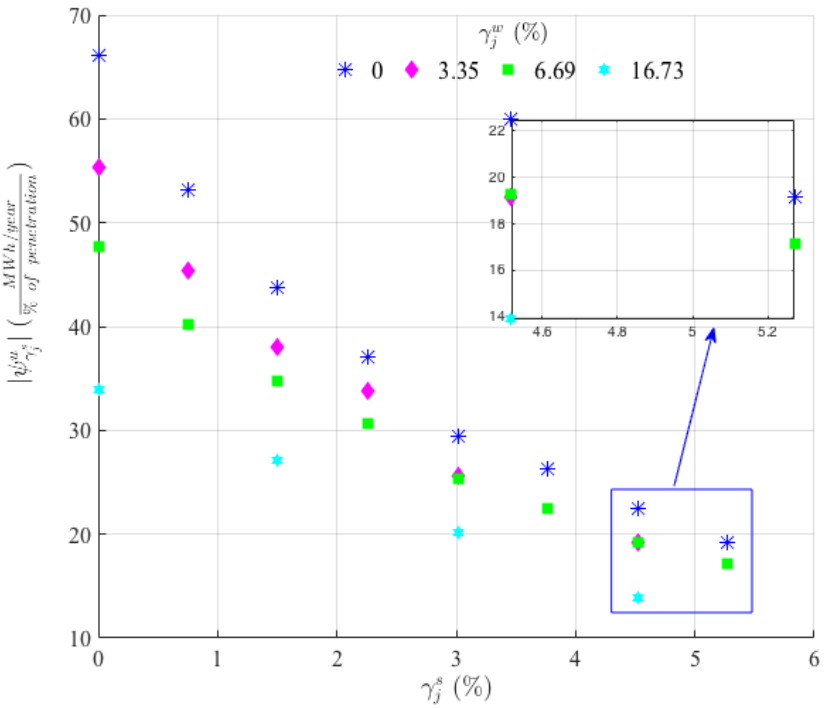

Figure 4.9: Sensitivity of the *EUE* metric with respect to solar generation penetration.

every 10 MW of integrated solar and wind generation capacity, 1 MW of conventional generation capacity is removed from the system. For example, the circle with center $[0, 28.4]^\dagger$ corresponds to the system with 0 MW integrated solar capacity and 15,000 MW of integrated wind capacity. The retirement fraction $\zeta_2 = 0.1$ allows the retirement of 1,500 MW conventional capacity. The plot indicates that for $\zeta_2 = 0.1$ the *LOLE* values decrease as we move in either direction, that increases solar or wind penetration. However, the decrease is more marked as we move from left to right for deeper values of solar penetrations than from bottom to top, i.e., deeper wind penetrations.

Our simulation studies further indicate that the decrease in the *LOLE* values for deeper wind penetrations, seizes to occur for $\zeta_i \geq 0.25$. Conventional capacity retirement at the fraction of 0.25 (0.5) means that for every 10 MW of integrated *RR* capacity, 2.5 MW (5 MW) of conventional capacity is retired. In these cases, the substitutability of retired generation by wind resources becomes so limited that the addition of multiples of the retired conventional capacity by wind resources is inadequate to maintain the "1

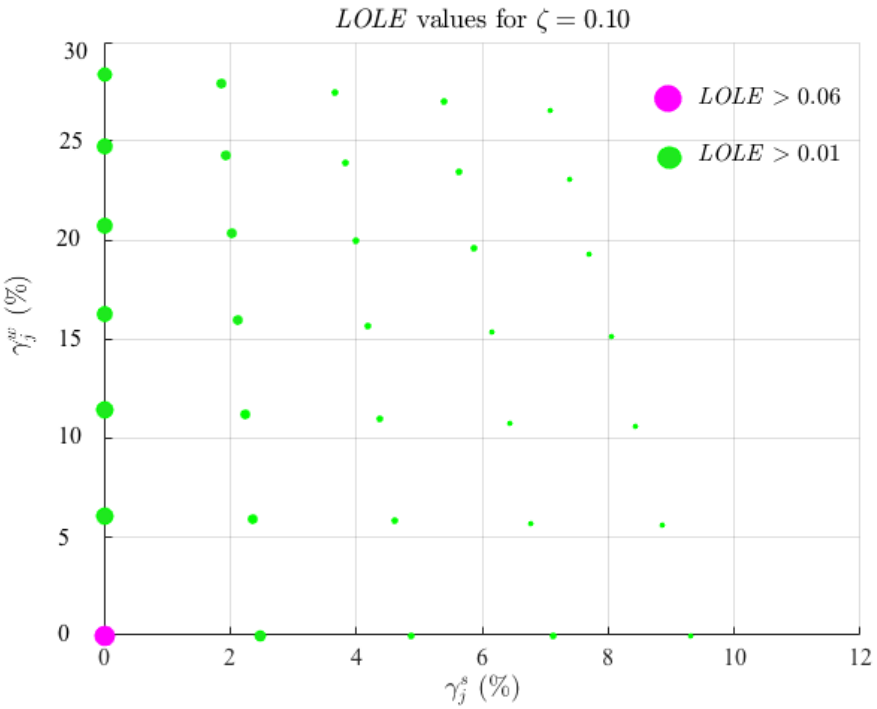

Figure 4.10: *LOLE* metric for 10% conventional generation retirement.

day in 10 years" criterion. We point out, however, that solar substitutability continues to maintain that criterion at both $\zeta_5 = 0.25$ and $\zeta_{10} = 0.50$ retirement fractions. This substitutability also reaches a limit for $\zeta_i \geq 0.75$ as illustrated in Figs. 4.13 and 4.14.

The behavior of the *LOLH* and *EUE* metric for $\zeta_{10} = 0.50$ are shown in Figs. 4.15 and 4.16 respectively.[4] We observe that for this value of the retirement fraction the substitutability of conventional capacity by wind resources is limited while solar resources continue to have a positive contribution to the resource adequacy of the study system. For $\zeta_{10} = 0.50$, the maximum (minimum) *LOLH* value is equal to 2 hours/year (0.164 hours/year) and corresponds to the case $[8.2,\ 30.7]^{\dagger}$ ($[5,\ 0]^{\dagger}$). The maximum (minimum) value for the *EUE* metric at 0.5 retirement fraction is found to be $3,962.1$ MWh/year (201.744 MWh/year) that corresponds to the case $[8.2,\ 30.7]^{\dagger}$ ($[9.7,\ 0]^{\dagger}$). In regard with the maximum values observed for the *LOLH* and *EUE* metrics for all the simulation cases, we found that those occur at 0.9 retirement

[4]The study results for each case with the analytical values of the *LOLE*, *LOLH* and *EUE* are available online at: https://github.com/Mariola-Nd/master-thesis-data.

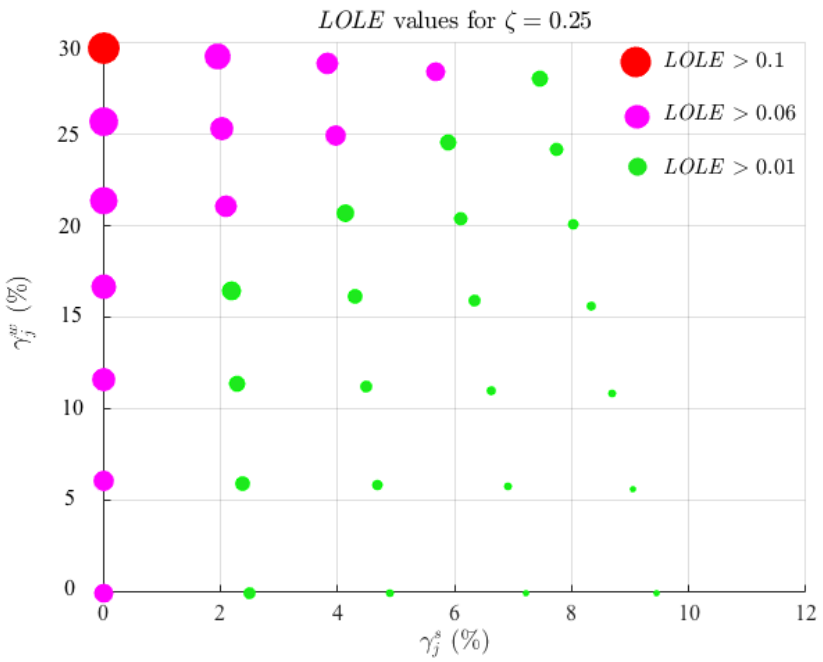

Figure 4.11: *LOLE* metric for 0.25 retirement fraction.

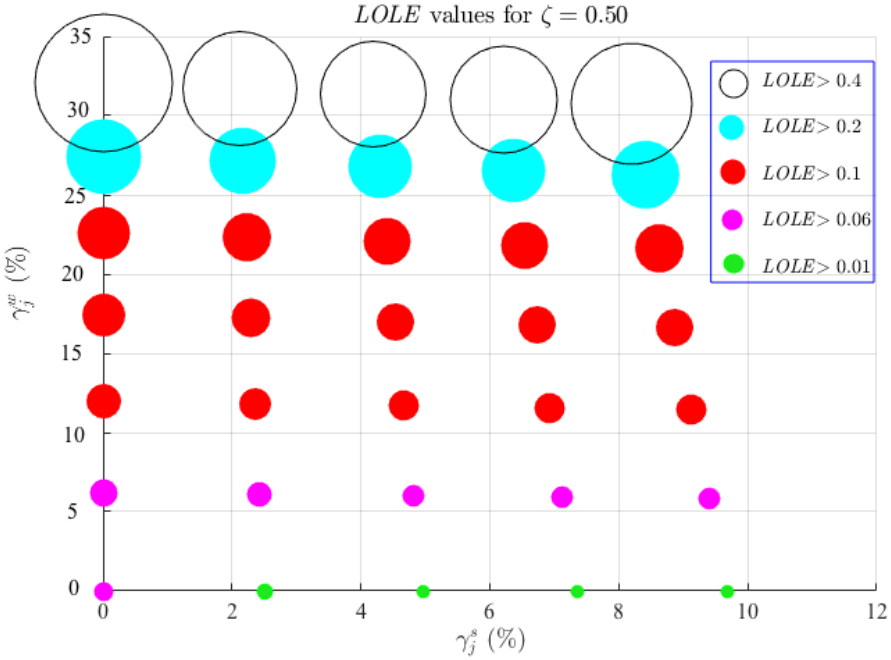

Figure 4.12: *LOLE* metric for 0.5 retirement fraction.

fraction and are equal to 34.25 hours/year and 50, 102.69 MWh/year, respectively. Both these values correspond to the case $[9.8,\ 30.7]^{\dagger}$ with $\zeta_{18} = 0.9$.

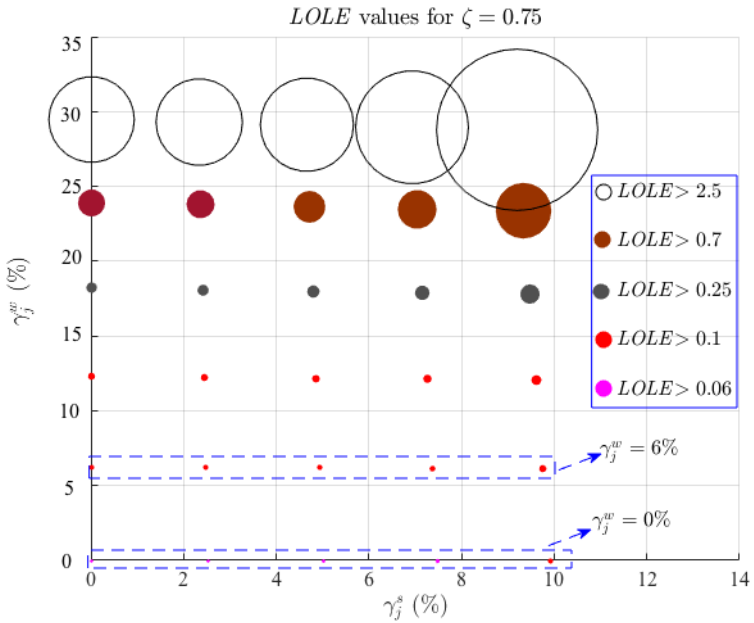

(a) $0\% \leq \gamma_j^w \leq 30\%$

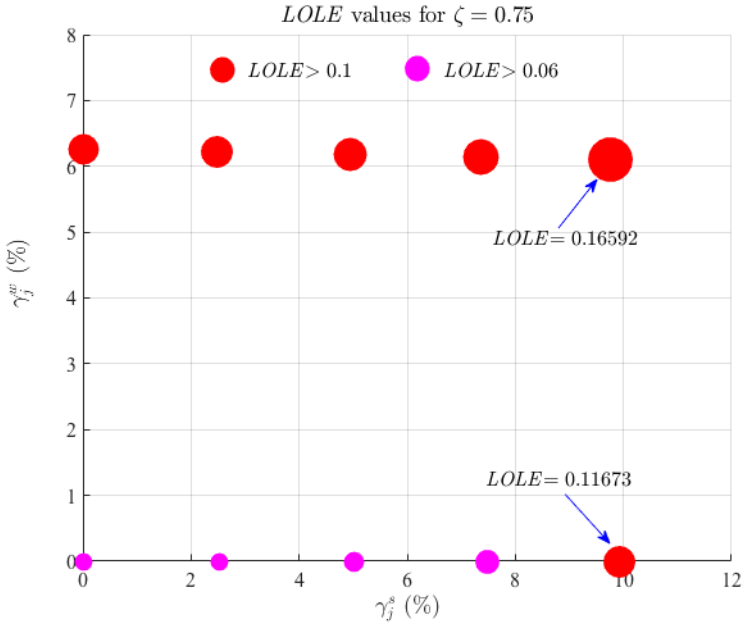

(b) $\gamma_j^w = 0\%$ and $\gamma_j^w = 6\%$

Figure 4.13: *LOLE* metric for 0.75 retirement fraction.

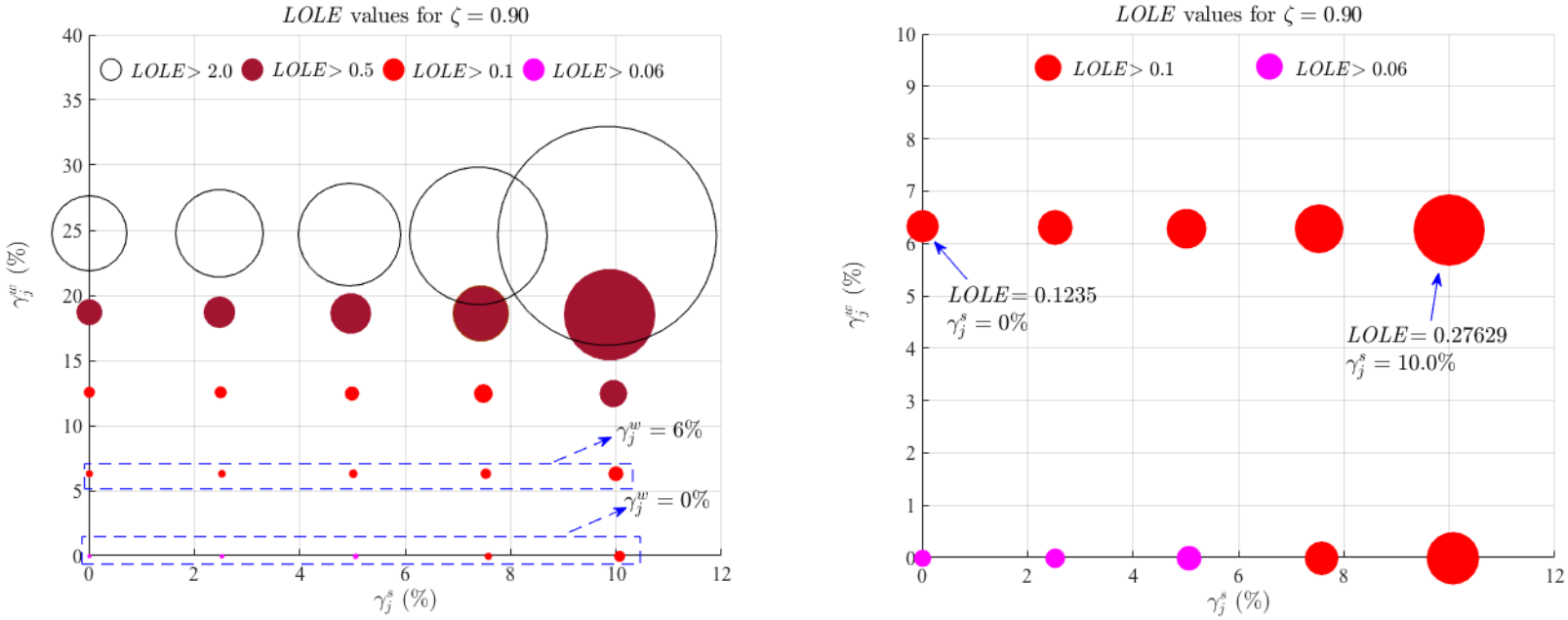

(a) $0\% \leq \gamma_j^w \leq 25\%$

(b) $\gamma_j^w = 0\%$ and $\gamma_j^w = 6\%$

Figure 4.14: *LOLE* metric for 0.9 retirement fraction.

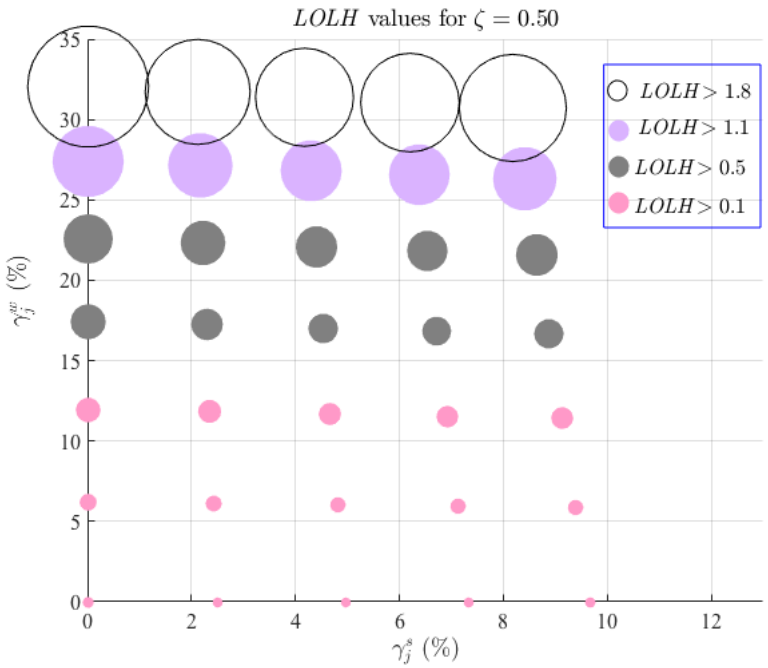

Figure 4.15: *LOLH* metric for 0.5 retirement fraction.

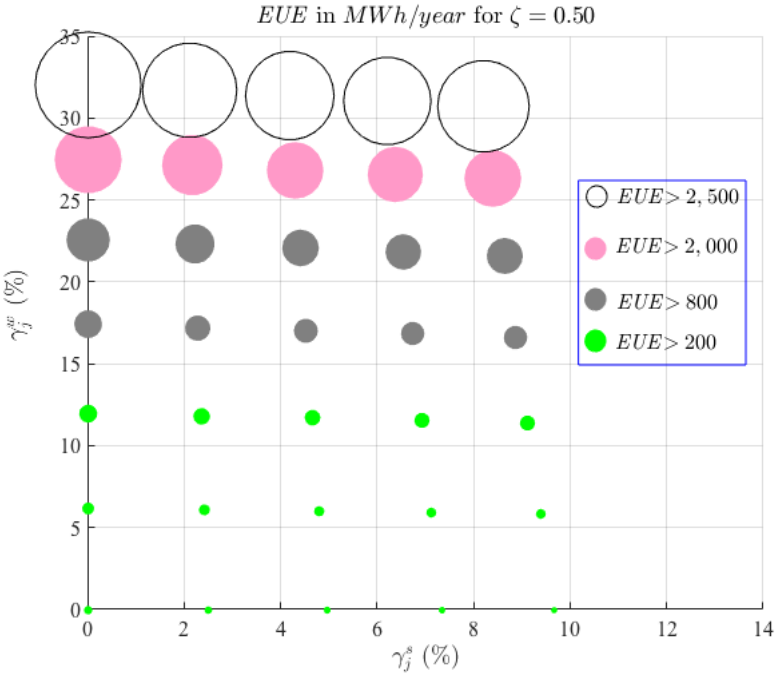

Figure 4.16: *EUE* metric for 0.5 retirement fraction.

4.4 Key findings from the studies

The study results presented in Sections 4.2 and 4.3 provide some very useful insights into the reliability impacts of deepening *RR* penetrations. The large-scale system with 37,500 MW of installed conventional and hydro resource capacity satisfies the "1 day in 10 years" resource adequacy criterion by itself. Clearly, the addition of solar and wind resource capacity can only improve the resource adequacy of the system as shown by the declining values of the metrics as the *RR* penetrations deepen. Indeed, for the study system, the *LOLE* drops from 0.06 days/year to 0.01 days/year when a total of 19,000 MW of solar and wind capacity is integrated into the system. Similar declines are also observed in the *LOLH* and *EUE* metrics that decrease from 0.18 hours/year to 0.025 hours/year and from 273 MWh/year to 20.8 MWh/year respectively.

For the fixed conventional resource mix, the impacts of the solar *RR*s appear to be significantly more pronounced than those of wind on the resource adequacy metrics. For example, with 500 MW (2,500 MW) of installed solar (wind) capacity for the study system, which result in 0.75% (3.35%) solar (wind) penetrations, the impact of solar (wind) capacity on the decrease of the *LOLE* is 23.15×10^{-3} (35.80×10^{-4}) day/year. Such results make sense because of the generally good and consistent tracking of the load by the solar generation during the peak summer months. On the other hand, the mismatch of the wind generation with the load is so consistent, that a five times greater capacity addition has an order of magnitude smaller impact on the *LOLE*. In terms of the days that 90% of the *LOLE* contributions come from the 10% peak load values, the hot summer days, when the load is close to or reaches its peak value, are the days or hours of day with the highest contribution to the *LOLE*. Consequently, deepening penetrations of solar generation have a more drastic impact on the resource adequacy metrics due to the closer tracking of load by solar resources. Therefore, the solar resources integrated into such systems, contribute significantly more to reduce the *LOLE* metric than wind as a function of the penetration level. The impacts of integrated solar *RR*s are similarly more marked on the *LOLH* and *EUE* metrics than those of wind *RR*s. However, the behavior of all the resource adequacy metrics is characterized by significant diminution of the marginal returns as the penetrations of solar and wind deepen. In effect,

when solar capacity increases from e.g., 0 MW to 500 MW, the declines in the resource adequacy metrics are significantly larger compared to the declines attained when solar capacity increases by the same amount from $3,500$ MW to $4,000$ MW. Similar behavior of the metrics is also exhibited by increased integrated capacities of wind resources.

The diminishing returns of deeper penetrations of solar and wind resources constitute limitations to the substitutability of retired conventional resource capacity by *RR*s. Our studies indicate that the retirement fraction ζ_i constitutes another limitation for the test system. Indeed, the studies in the test system indicate that the declining effect of both wind and solar *RR*s on the *LOLE* metric persists until the limiting value $\zeta_2 = 0.1$. For $0.1 < \zeta_i \leq 0.50$, while the declining effect of solar continues to exists, the deepening penetrations of wind appear to increase the *LOLE* values. To understand such outcomes that highlight the distinct behavior of wind and solar resources, we need to consider two important aspects of the study. First, the step at which we gradually integrate solar capacity in the system for each case is equal to 500 MW, while for wind is $1,250$ MW. This implies that as wind penetrations deepen, the retired conventional capacity in MW value is greater than when solar panetrations deepen, although the overal retirement ratio stays the same. For example, assume a case c_j with $\kappa_j^s = 500$ MW and $\kappa_j^w = 1,250$ MW. A retirement fraction of $\zeta_5 = 0.25$ implies that 437.5 MW of conventional capacity are replaced by $1,750$ MW of *RR* capacity. If we increase the wind capacity by a single step we move to the case $c_{j'}, j' \neq j$ with $\kappa_{j'}^w = 2,500$ MW and $\kappa_{j'}^s = 500$ MW. For a retirement fraction $\zeta_5 = 0.25$ the total retired conventional capacity is now equal to 750 MW. If from the case c_j we wish to increase the solar capacity by a single step, we move to the case $c_{\hat{j}}$, $\hat{j} \neq j$, with $\kappa_{\hat{j}}^w = 1,250$ MW and $\kappa_{\hat{j}}^s = 1,000$ MW. In this case, the replaced conventional capacity is equal to 562.5 MW. As such, more conventional generation capacity is retired as we move to deeper wind than solar penetrations. The second aspect is again related to the closer tracking of the load by the solar *RR*s as evidenced by the declines of the metric values as solar penetrations deepen.

The tracking ability of solar resources during the peak summer months is limited for $0.75 \leq \zeta_i \leq 0.9$. Indeed, as illustrated in the Figs. 4.13 and 4.14 the *LOLE* metric increases rapidly with both solar and wind generation penetrations. We note that for $\zeta_{18} = 0.9$, although we start with

a resource adequate system that satisfies $LOLE < 0.1$ days/year, we end up with $LOLE > 2$ days/year. More specifically, at 19,000 MW of total installed wind and solar capacity and 17,100 MW retired conventional capacity, the $LOLE \backsimeq 6.0$ days/year. Such limitations on RR substitutability for retired conventional capacity require careful attention from grid operators. The approach used in the studies makes effective use of the framework to facilitate the development of appropriate retirement schedules that have acceptable resource adequacy characteristics.

4.5 Conclusions

In this chapter we presented representative results from our extensive application studies on a realistic large-scale system with total installed capacity of 40,000 MW and projected summer peak load 36,800 MW. The study results provide quantifications of the behavior of the resource adequacy metrics with respect to deepening solar and wind penetrations. For a fixed set of conventional supply resources, the deepening RR penetrations have a major contribution to the improvement of the resource adequacy, as evidenced by the declining values of the metrics. More specifically, the results demonstrate the significantly more marked impacts of solar resources to the resource adequacy of the system compared to those of wind resources. Furthermore, we observe the diminution of the marginal returns in each metric for deepening penetrations of both solar and wind generation. When the retirement of conventional capacity is taken into consideration, the substitutability of conventional resources by wind RRs becomes limited for retirement fractions $\zeta_i \geq 0.25$. Solar resources, however, are capable to effectively substitute the retired conventional capacity up to the limiting retirement fraction value $\zeta_{10} = 0.5$. For values of $\zeta_i > 0.5$ neither solar or wind integrated capacity is capable to efficiently substitute the retired conventional capacity and thus resulting in values of the resource adequacy metrics well above the acceptable standards.

CHAPTER 5

CONCLUDING REMARKS

The breakthroughs in technology and the environmental concerns over the climate change are the key drivers in the wider implementation of *RR*s everywhere. This thesis focuses on the important aspect of resource adequacy to study the impacts of the deepening penetrations of *RR* generation in the grid's reliability and the quantification of these impacts for wind and solar *RR*s in particular. We start out with a review of the conventional time-abstracted resource adequacy assessment framework, which we view as the mechanism to define and evaluate the industry-wide reliability metrics on a consistent basis. These metrics include the *LOLP*, *LOLH*, *LOLE* and the *EUE*. We use the time-abstracted framework to provide the analytical expressions of the metrics and discuss their salient characteristics in order to clarify various misconceptions associated with the metrics interpretation.

The limitations of the time-abstracted framework in the incorporation of the intermittent and time-varying nature of *RR*s motivated the development of a simulation-based, time-dependent resource adequacy framework with the capability to represent the uncertain and time-varying nature of loads and demand/supply resources, including the intermittency in the outputs of *RR*s. In this framework, the loads, supply/demand resources and *RR*s are modeled as stochastic processes with sample paths (*s.p.*s) constructed from historical data. Such representation effectively incorporates the spatial and chronological correlations among the *s.p.*s of the loads, the supply/demand resources and the *RR*s. The *RR*s in the system are incorporated via the net load, whose sample space is constructed from load and *RR* data from the same time period to ensure that the weather correlation between loads and *RR*s is taken into consideration. To evaluate the resource adequacy metrics, we derive the analogues of the analytical expressions of the metrics in the time-dependent framework. Furthermore, the implementation of the framework provides additional degrees of freedom for the definition and evaluation of

new metrics that are particularly appropriate for the study at hand. As such, we develop new sensitivity indices to quantify the marginal behavior of each resource adequacy metric with respect to the deepening RR penetrations.

The effectiveness of the time-dependent framework is demonstrated via its extensive applications to evaluate the resource adequacy of large-scale study systems. In the studies, we characterize the impacts of deepening RR penetrations on the resource adequacy through the behavior of the evaluated metrics — $LOLH$, $LOLE$ and EUE. Given the non-negative output of RRs, the net load $s.p.$s are bounded above by the system load $s.p.$s, resulting in the decrease of all the metrics. Solar and wind RRs appear to have distinct impacts on the metrics, with solar contributing significantly more to the reduction of the $LOLE$ than wind, as a function of the RR penetration level. Another important finding is the diminishing marginal returns characteristic on each metric associated with the deepening wind and solar penetrations. More specifically, the improvement on the system's resource adequacy becomes minuscule for integrated solar and wind capacities greater than $2,000\,\text{MW}$ and $7,500\,\text{MW}$ respectively.

The extensive resource adequacy studies we conducted are useful not only in illustrating the nature of the behavior of the metrics with deepening RR penetrations but also for the quantified assessment of the substitutability of the conventional generation resources by RRs. More specifically, we observe that notwithstanding deepening RR penetrations, the resource adequacy of the study system begins to deteriorate, i.e., increasing values of metrics, with the conventional generation retirement. In fact, for conventional retirement fraction greater than 0.25, the inability of the grid to meet the "1 day in 10 years" resource adequacy criterion becomes evident. The increase in the number of violations of the "1 day in 10 years" criterion is notably marked for retirement fraction values at 0.75 and 0.9, with $LOLE$ below 0.1 days/year only for a limited number of cases. Such results demonstrate the limited ability of RRs in the provision of resource adequacy and highlight the care that grid operators must exercise in the retirement of fossil-fired units. A particularly interesting finding is that for conventional retirement fractions greater than 0.25, the integration of $15,000\,\text{MW}$ wind and $0\,MW$ solar capacity appears as the worst planning strategy as evidenced by the escalating values of all the resource adequacy metrics. In fact, the studies indicate that any conventional resource retirement schedule that is not coupled with the

integration of solar capacity, but rather focuses entirely on wind resources, results in significant deterioration in the grid's resource adequacy. The *LOLH* and *EUE* metrics increase rapidly with the wind penetration at 0.5 conventional retirement fraction. At the same time, solar resources continue to influence the indices in the opposite, i.e., decreasing, direction. However, the positive influence of solar generation vanishes at higher values of the retirement fraction. It is difficult to conclude at which values of conventional retirement fractions and for which cases the study system is resource inadequate, since there do not exist widely accepted criteria expressed in terms of the *LOLH* or *EUE* metrics. *NERC* has long called for "more widely-adopted energy-related reliability metrics and targets as the share of variable generation increases in the power systems"[10] and such metrics are already being used in various parts of the world [3]. However, in this study we focus on the "1 day in 10 years" resource adequacy standard, yet the usefulness and appropriateness of this standard are out of the scope of our studies. The question of whether the *EUE* and *LOLH* metrics are more appropriate for setting resource adequacy criteria than the *LOLE* as well as the introduction of entirely new metrics that are appropriate for systems with high *RR* penetrations, are interesting topics of further research.

In the time-dependent framework discussed in this thesis the integration of *RR*s to the existing fleet of conventional resources is expected to have a non-negative contribution to the grid's resource adequacy given the non-negative outputs of *RR*s. In terms of the overall coupled effects of the deepening *RR* penetrations and conventional capacity retirement, we cannot establish general conclusions for every study system. The conclusions that we draw depend on the characteristics of the loads, demand/supply resources as well as the integrated *RR* capacities in each case for the particular study at hand. For example, in a winter-peaking system we may not observe the marked contributions of solar *RR*s to resource adequacy reported here and furthermore, the impact of wind generation may be more pronounced.

There are a number of extensions of the work presented here. The time-dependent framework described in this thesis is sufficiently general to allow the respresentation of various other resources such as *DRR*s or other technology type groups of *RR*s. In the modeling area, the simulation-based framework described in this thesis assumes that the network is 100 % available and congestion-free. As such, the metric values derived in the studies do not

incorporate the probability that a $\ell.o.\ell.$ event may occur due to the fact that the grid is incapable to deliver the power supply to the loads. Therefore, a key topic of interest is the incorporation of the network effects in the resource adequacy evaluation. The presence of congestion in the network or failures on the transmission lines may prevent the delivery of power from the supply resources to the loads, even if there exists sufficient available generation capacity. In this regard, the impacts of possible line failures and congestion need to be taken into consideration. This work requires both analytic development and computational implementation. In addition, the modeling of the network is critical to allow the respresentation of distributed energy resource aggregations that are starting to play an increasingly significant role in bulk power systems.

APPENDIX A

LOLP EVALUATION MECHANICS

In this appendix we provide an analytical computation of the *LOLP* for a system with G conventional generation units. Based on the general expression (2.4), we explicitly make use of conditional probability and assumptions $A\,2$ and $A\,3$ to derive two equivalent alternative approaches to calculate the *LOLP*.

The first approach is based on the combination of exact generation capacity states with cumulative demand levels [6]. Cumulative demand levels can be obtained from the *LDC*. The *LOLP* can be viewed as the probability that the system demand is strictly greater than any available capacity state of the supply resources. For the system with J distinct available capacity states, if we condition on the event of being in each state a_j, then (2.3) can be rewritten as

$$\rho = \sum_{j=1}^{J} \mathbb{P}\left\{ \underset{\sim}{L} > a_j \middle| \underset{\sim}{A}_T = a_j \right\} \mathbb{P}\left\{ \underset{\sim}{A}_T = a_j \right\}. \tag{A.1}$$

In (A.1) the first term can be rewritten as $\mathbb{P}\left\{ \underset{\sim}{L} > a_j \right\}$ (due to assumption $A\,2$) and is obtained from the *LDC*: for a demand level equal to a_j the abscissa indicates the fraction of time, i.e., the probability, that demand exceeds the value a_j. The terms $\mathbb{P}\left\{ \underset{\sim}{A}_T = a_j \right\}$ for $j = 1, \ldots, J$, are the state probabilities p_j.

The second approach to evaluate the *LOLP* is based on distinct demand levels and cumulative available generation capacity states. In this scheme, we condition on the event of being at each demand level. We assume there exist $\widetilde{H} \leq H$ hours with distinct demand levels. We denote the set of such hours by the subset $\mathscr{H} \subseteq \mathscr{T}_h$ and define it as $\mathscr{H} = \{h : \ell_h \neq \ell_{h'}\ \forall h, h' \in \mathscr{T}_h, h \neq h'\}$. Each demand level ℓ_h for $h \in \mathscr{H}$, has an associated probability of occurrence equal to the ratio of the total number of times ℓ_h appears in the sample space

of $\underset{\sim}{L}$ divided by the cardinality of the sample space, i.e., H. If we denote the total number of occurrences of ℓ_h by ω_h, then the probability of ℓ_h is equal to $\dfrac{\omega_h}{H}$, for $h \in \mathscr{H}$ and $\omega_h \geq 1$. The *LOLP* is defined as the probability that the total available generation capacity is strictly less than any demand level, or in mathematical terms

$$\rho = \sum_{h \in \mathscr{H}} \mathbb{P}\left\{ \underset{\sim}{A}_T < \ell_h \middle| \underset{\sim}{L} = \ell_h \right\} \mathbb{P}\left\{ \underset{\sim}{L} = \ell_h \right\} \ . \tag{A.2}$$

We define the loss of load probability function $\phi(\cdot)\colon \mathbb{R}_+ \to [0,1]$ as $\phi(\ell_h) = \mathbb{P}\left\{ \underset{\sim}{A}_T < \ell_h \right\}$ to represent the probability of $\ell.o.\ell.$ at any load level ℓ_h. Therefore, we can rewrite (A.2) as

$$\rho = \sum_{h \in \mathscr{H}} \phi(\ell_h) \ \frac{\omega_h}{H} \ . \tag{A.3}$$

In order to calculate the values of $\phi(\ell_h)$, we need to derive an expression of the *c.d.f.* of the *r.v.* $\underset{\sim}{A}_T$. Under the assumption $A3$ and making use of the convolution formula we write,

$$\begin{aligned}
\mathbb{P}\left\{ \sum_{k=1}^{G} \underset{\sim}{A}_k \leq \ell_h \right\} &= \mathbb{P}\left\{ \sum_{k=1}^{G-1} \underset{\sim}{A}_k \leq \ell_h \middle| \underset{\sim}{A}_G = 0 \right\} \mathbb{P}\left\{ \underset{\sim}{A}_G = 0 \right\} \\
&+ \mathbb{P}\left\{ \sum_{k=1}^{G-1} \underset{\sim}{A}_k \leq \ell_h - d_G^1 \middle| \underset{\sim}{A}_G = d_G^1 \right\} \mathbb{P}\left\{ \underset{\sim}{A}_G = d_G^1 \right\} \\
&+ \mathbb{P}\left\{ \sum_{k=1}^{G-1} \underset{\sim}{A}_k \leq \ell_h - d_G^2 \middle| \underset{\sim}{A}_G = d_G^2 \right\} \mathbb{P}\left\{ \underset{\sim}{A}_G = d_G^2 \right\} \\
&+ \ldots + \mathbb{P}\left\{ \sum_{k=1}^{G-1} \underset{\sim}{A}_k \leq \ell_h - c_G \middle| \underset{\sim}{A}_G = c_G \right\} \mathbb{P}\left\{ \underset{\sim}{A}_G = c_G \right\} \qquad \text{(A.4)} \\
= \mathbb{P}\left\{ \sum_{k=1}^{G-1} \underset{\sim}{A}_k \leq \ell_h \right\} \left[1 - \sum_{j=1}^{n-2} r_G^j - p_G \right] &+ \mathbb{P}\left\{ \sum_{k=1}^{G-1} \underset{\sim}{A}_k \leq \ell_h - c_G \right\} p_G \\
+ \sum_{j=1}^{n-2} \mathbb{P}\left\{ \sum_{k=1}^{G-1} \underset{\sim}{A}_k \leq \ell_h - d_G^j \right\} (r_G^j) &= F_{\underset{\sim}{A}_{T/g_G}}(\ell_h) \left[1 - \sum_{j=1}^{n-2} r_G^j - p_G \right] \\
&+ F_{\underset{\sim}{A}_{T/g_G}}(\ell_h - c_G)\ p_G + \sum_{j=1}^{n-2} F_{\underset{\sim}{A}_{T/g_G}}(\ell_h - d_G^j)\ r_G^j \ ,
\end{aligned}$$

where

$$\underset{\sim}{A}_{T/g_G} = \sum_{k=1}^{G-1} \underset{\sim}{A}_k \ . \tag{A.5}$$

The application of the convolution formula enables the construction of a powerful recursive technique that may be used to evaluate the *c.d.f.* of the sum of any finite number of available capacity *r.v.*s. The impact of the addition of a new n-state generation unit, with $n \geq 2$, on the *LOLP*, is determined by conditioning on the unit being in any of its n possible states. Thus, we derive a final expression of the *c.d.f.* of the G units that depends on the state probabilities of unit g_G and on the *c.d.f.* values of the sum of available capacities of the $G-1$ units, whose computation is iteratively done. In this way, the probability of loss of load for the entire period $\mathscr{T}_h$ is based on the evaluation of the *LOLP* at each demand level ℓ_h weighted by the probabilities of ℓ_h.

Alternatively, we can evaluate the *LOLP* through the conduction of H independent experiments, one for each hour in the period, where the cumulative available capacity states are compared with the hourly demand value. In this approach, we condition on the event of being at each hour h in the period. For each $h \in \mathscr{T}_h$, we examine whether for a given single demand level for the entire hour, the total available generation capacity is sufficient to meet that demand — the no $\ell.o.\ell.$ condition. Everytime we condition on the event of being in any hour $h \in \mathscr{T}_h$, the demand *r.v.* takes the corresponding value ℓ_h in that hour. Hence, we can evaluate the *LOLP* as

$$\rho = \sum_{h=1}^{H} \mathbb{P}\left\{ \underset{\sim}{A}_T < \ell_h \middle| hour\ h \right\} \mathbb{P}\left\{ hour\ h \right\} \ . \tag{A.6}$$

Note that in (A.5) the conditional probabilities are the values of $\phi(\ell_h)$ since the events $\{hour\ h\}$ and $\left\{ \underset{\sim}{A}_T < \ell_h \right\}$ are assumed statistically independent. The weights of $\phi(\ell_h)$ are the probabilities of being in every hour h. Under the assumption that the events of being in any hour h, for each $h \in \mathscr{T}_h$, are equiprobable,

$$\rho = \frac{1}{H} \sum_{h=1}^{H} \phi(\ell_h) \ . \tag{A.7}$$

Equations (A.3) and (A.7) yield exactly the same values for ρ. The subtlety

is that in the first scheme we condition on the events of being at each distinct demand level ℓ_h, which are not equiprobable since $|\mathscr{H}| \leq |\mathscr{T}_h|$.

APPENDIX B

PROOF OF THE INEQUALITIES (2.12)

In this appendix we provide a proof for the inequalities (2.12). Without any loss of generality we can assume $\mathscr{T}_d$ to consist of a single day $\{d_1\}$ and $\mathscr{T}_h = \{h_1, h_2, \ldots, h_{24}\}$. In this case $\xi_{\mathscr{T}_d}$ is given by

$$\xi_{\mathscr{T}_d} = \phi(\ell_{d_1}) \; \frac{days}{1 \; day} \; , \tag{B.1}$$

where $\ell_{d_1} = \max\{\ell_{h_1}, \ell_{h_2}, \ldots, \ell_{h_{24}}\} = \ell_{h_p}$ with h_p denoting the peak load hour of day d_1. For the computation of $\eta_{\mathscr{T}_h}$,

$$\begin{aligned} \eta_{\mathscr{T}_h} &= \sum_{k=1}^{24} \phi(\ell_{h_k}) = \phi(\ell_{h_1}) + \phi(\ell_{h_2}) +, \ldots, +\phi(\ell_{h_p}) +, \ldots, +\phi(\ell_{h_{24}}) \\ &= \phi(\ell_{h_1}) + \phi(\ell_{h_2}) +, \ldots, +\xi_{\mathscr{T}_d} +, \ldots, +\phi(\ell_{h_{24}}) \; \frac{hours}{24 \; hours} \geq \xi_{\mathscr{T}_d} \; , \end{aligned} \tag{B.2}$$

since $\phi(\ell_{h_k})$ are non-negative quantities. We can restrict the maximum value of $\xi_{\mathscr{T}_d}$ if we take the maximum value of $\phi(\ell_{h_k})$ in the period, which corresponds to the peak hourly load

$$\begin{aligned} \eta_{\mathscr{T}_h} &= \sum_{k=1}^{24} \phi(\ell_{h_k}) \; \frac{hours}{24 \; hours} \leq \sum_{k=1}^{24} \phi(\ell_{h_p}) \; \frac{hours}{24 \; hours} \\ &= 24 \; \phi(\ell_{h_p}) \; \frac{hours}{24 \; hours} = 24 \; \xi_{\mathscr{T}_d} \; . \end{aligned} \tag{B.3}$$

From inequalities (B.2) and (B.3) we arrive to

$$\xi_{\mathscr{T}_d} \leq \eta_{\mathscr{T}_h} \leq 24 \; \xi_{\mathscr{T}_d} \; . \tag{B.4}$$

APPENDIX C

STUDY RESULTS

Table C.1: Resource adequacy metrics for wind and solar capacity integrations for cases c_1 to c_{13}.

c_j	ξ (days/year)	η (hours/year)	u (MWh/year)
c_1	0.06034	0.18178	273.024
c_2	0.05272	0.16227	255.222
c_3	0.04669	0.14618	239.783
c_4	0.04131	0.13278	226.857
c_5	0.03676	0.12089	214.943
c_6	0.03319	0.11145	204.216
c_7	0.03018	0.10372	195.087
c_8	0.02799	0.09726	187.121
c_9	0.02601	0.09149	179.258
c_{10}	0.02331	0.08329	166.991
c_{11}	0.02145	0.0767	155.108
c_{12}	0.04293	0.13818	223.261
c_{13}	0.03666	0.12303	209.815

Table C.2: Resource adequacy metrics for wind and solar capacity integrations for cases c_{14} to c_{31}.

c_j	ξ (days/year)	η (hours/year)	u (MWh/year)
c_{14}	0.03164	0.11031	198.164
c_{15}	0.02778	0.10034	188.294
c_{16}	0.02525	0.09242	179.034
c_{17}	0.02941	0.10583	183.313
c_{18}	0.02555	0.09514	172.999
c_{19}	0.02244	0.08631	164.023
c_{20}	0.02032	0.07956	156.24
c_{21}	0.01894	0.07415	148.79
c_{22}	0.01733	0.06635	136.099
c_{23}	0.01618	0.06068	125.103
c_{24}	0.01566	0.05691	115.984
c_{25}	0.01514	0.05352	107.184
c_{26}	0.02121	0.08327	150.351
c_{27}	0.01909	0.07582	142.299
c_{28}	0.01754	0.0699	135.465
c_{29}	0.01682	0.06582	128.823
c_{30}	0.01612	0.06173	122.668
c_{31}	0.01707	0.0678	122.31

Table C.3: Resource adequacy metrics for wind and solar capacity integrations for cases c_{32} to c_{49}.

c_j	ξ (days/year)	η (hours/year)	u (MWh/year)
c_{32}	0.01612	0.06305	115.79
c_{33}	0.01554	0.0592	109.907
c_{34}	0.01517	0.05621	104.605
c_{35}	0.01498	0.05372	99.408
c_{36}	0.01456	0.0513	95.123
c_{37}	0.01443	0.04968	90.69
c_{38}	0.01435	0.04844	86.542
c_{39}	0.01419	0.04688	82.409
c_{40}	0.01389	0.0444	74.986
c_{41}	0.01354	0.04221	68.372
c_{42}	0.01508	0.05786	100.176
c_{43}	0.01423	0.04766	80.347
c_{44}	0.01436	0.05103	80.367
c_{45}	0.01394	0.04611	71.322
c_{46}	0.01383	0.04318	63.413
c_{47}	0.0137	0.04087	56.471
c_{48}	0.01334	0.03835	50.231
c_{49}	0.01276	0.03628	44.57

Table C.4: Resource adequacy metrics for wind and solar capacity integrations for cases c_{50} to c_{59}.

c_j	ξ (days/year)	η (hours/year)	u (MWh/year)
c_{50}	0.01216	0.03417	39.886
c_{51}	0.01389	0.04505	63.452
c_{52}	0.01354	0.03875	48.914
c_{53}	0.01359	0.03981	48.931
c_{54}	0.01349	0.03683	42.358
c_{55}	0.01338	0.03429	35.922
c_{56}	0.01293	0.03195	31.102
c_{57}	0.01215	0.02934	26.971
c_{58}	0.01135	0.0269	23.601
c_{59}	0.01055	0.02461	20.805

Table C.5: Sensitivity indices of the *LOLE* and *LOLH* with respect to wind penetration for cases c_1 to c_4.

$\underline{\boldsymbol{\gamma}}_0^\dagger$	$\delta\gamma_j^w$	$\left.\frac{\psi^{\xi}_{\gamma_j^w}}{\%\ of\ penetration}\right\vert_{\underline{\boldsymbol{\gamma}}_0}$ $days/year$	$\left.\frac{\psi^{\eta}_{\gamma_j^w}}{\%\ of\ penetration}\right\vert_{\underline{\boldsymbol{\gamma}}_0}$ $hours/year$
[0 0]	1.66788	-0.00457	-0.01170
[0 1.67]	1.68429	-0.00358	-0.00955
[0 3.35]	1.67274	-0.00322	-0.00801
[0 5.02]	1.66220	-0.00274	-0.00715

Table C.6: Sensitivity indices of the *LOLE* and *LOLH* with respect to wind penetration for cases c_5 to c_{21}.

$\underline{\gamma}_0^{\dagger}$	$\delta\gamma_j^w$	$\psi^{\xi}_{\gamma_j^w}\Big\vert_{\underline{\gamma}_0}$ $\frac{days/year}{\%\ of\ penetration}$	$\psi^{\eta}_{\gamma_j^w}\Big\vert_{\underline{\gamma}_0}$ $\frac{hours/year}{\%\ of\ penetration}$
[0 6.69]	1.66788	-0.00214	-0.00566
[0 8.35]	1.68429	-0.00179	-0.00459
[0 10.04]	1.67274	-0.00131	-0.00386
[0 11.71]	1.66222	-0.00119	-0.00347
[0 13.37]	3.35575	-0.00080	-0.00244
[0 16.73]	3.33000	-0.00056	-0.00198
[1.50 0]	1.66788	-0.00231	-0.00641
[1.50 1.67]	1.68429	-0.00185	-0.00524
[1.50 3.35]	1.67274	-0.00127	-0.00404
[1.50 5.02]	1.66220	-0.00083	-0.00325
[1.50 6.69]	3.35218	-0.000480	-0.00233
[1.50 10.04]	3.33496	-0.000345	-0.00170
[1.50 13.37]	3.35575	-0.00015	-0.00112
[1.50 16.73]	3.33000	-0.00016	-0.00102
[3.01 0]	1.66788	-0.00057	-0.00285
[3.01 1.67]	1.68429	-0.00034	-0.00228
[3.01 3.35]	1.67274	-0.00022	-0.00179

Table C.7: Sensitivity indices of the *LOLE* and *LOLH* with respect to wind penetration for cases c_{22} to c_{38}.

$\underline{\boldsymbol{\gamma}}_0^{\dagger}$	$\delta\gamma_j^w$	$\psi^{\xi}_{\gamma_j^w}\Big\vert_{\underline{\boldsymbol{\gamma}}_0}$ $\frac{days/year}{\%\ of\ penetration}$	$\psi^{\eta}_{\gamma_j^w}\Big\vert_{\underline{\boldsymbol{\gamma}}_0}$ $\frac{hours/year}{\%\ of\ penetration}$
[3.01 5.02]	1.66220	-0.00011	-0.00150
[3.01 6.69]	1.66788	-0.00025	-0.00145
[3.01 8.35]	1.68429	-7.71836×10^{-5}	-0.00096
[3.01 10.04]	1.67274	-4.78257×10^{-5}	-0.00074
[3.01 11.71]	1.66222	-9.62569×10^{-5}	-0.00094
[3.01 13.37]	3.35575	-8.93988×10^{-5}	-0.00074
[3.01 16.73]	3.33000	-0.00011	-0.00066
[4.52 0]	3.35217	-0.00013	-0.00147
[4.52 3.35]	3.33494	-3.29841×10^{-5}	-0.00088
[4.52 6.69]	3.35218	-3.87808×10^{-5}	-0.00069
[4.52 10.04]	3.33496	-0.00011	-0.00076
[4.52 13.37]	3.35575	-0.00017	-0.00062
[4.52 16.73]	3.33000	-0.00018	-0.00063
[6.03 0]	3.35217	-2.98314×10^{-5}	-0.00089
[6.03 3.35]	3.33494	-3.29841×10^{-5}	-0.00076
[6.03 6.69]	3.35218	-0.00013	-0.00070
[6.03 10.04]	3.33496	-0.00023	-0.00078

Table C.8: Sensitivity indices of the *LOLE* and *LOLH* with respect to solar penetration for cases c_1 to c_{17}.

$\underline{\gamma}_0^\dagger$	$\delta\gamma_j^s$	$\psi^{\xi}_{\gamma_j^s}\Big\vert_{\underline{\gamma}_0}$ $\frac{days/year}{\%\ of\ penetration}$	$\psi^{\eta}_{\gamma_j^s}\Big\vert_{\underline{\gamma}_0}$ $\frac{hours/year}{\%\ of\ penetration}$
[0 0]	0.75199	-0.02315	-0.05798
[0.75 0]	0.75220	-0.01797	-0.04300
[1.50 0]	0.75235	-0.01090	-0.02999
[2.26 0]	0.75759	-0.00546	-0.02057
[3.01 0]	0.75199	-0.00265	-0.01322
[3.76 0]	0.75221	-0.00096	-0.00908
[4.51 0]	0.75235	-0.00062	-0.00795
[5.27 0]	0.75759	-0.00040	-0.00692
[0 3.35]	0.75199	-0.02001	-0.04770
[0.75 3.35]	0.75220	-0.01223	-0.03191
[1.50 3.35]	0.75235	-0.00651	-0.02181
[2.25 3.35]	0.75759	-0.00264	-0.01412
[3.01 3.35]	1.50420	-0.00106	-0.00870
[4.51 3.35]	1.50994	-0.00030	-0.00614
[0 6.69]	0.75199	-0.01531	-0.03786
[0.75 6.69]	0.75220	-0.00839	-0.02429
[1.50 6.69]	0.75235	-0.00375	-0.01651

Table C.9: Sensitivity indices of the *LOLE* and *LOLH* with respect to solar penetration for cases c_{18} to c_{28}.

$\underline{\boldsymbol{\gamma}}_0^\dagger$	$\delta\gamma_j^s$	$\psi^{\xi}_{\gamma_j^s}\Big\vert_{\underline{\boldsymbol{\gamma}}_0}$ $\frac{days/year}{\%\ of\ penetration}$	$\psi^{\eta}_{\gamma_j^s}\Big\vert_{\underline{\boldsymbol{\gamma}}_0}$ $\frac{hours/year}{\%\ of\ penetration}$
[3.01 6.69]	0.75199	-0.00100	-0.00806
[3.76 6.69]	0.75221	-0.00053	-0.00596
[4.52 6.69]	0.75235	-0.00039	-0.00589
[0 16.73]	1.50419	-0.00509	-0.01754
[1.50 16.73]	1.50994	-0.00117	-0.00829
[3.01 16.73]	1.504196	-0.00075	-0.00539
[4.52 16.73]	1.50994	-0.00093	-0.00621
[0 20.06]	1.50419	-0.00419	-0.01541
[1.50 20.06]	1.50994	-0.00106	-0.00749
[3.01 20.06]	1.50420	-0.00092	-0.00534
[4.52 20.06]	1.50994	-0.00106	-0.00633

Table C.10: Sensitivity indices of the *EUE* with respect to wind penetration for cases c_1 to c_3.

$\underline{\boldsymbol{\gamma}}_0^\dagger$	$\delta\gamma_j^w$	$\psi^{u}_{\gamma_j^w}\Big\vert_{\underline{\boldsymbol{\gamma}}_0}$ $\frac{MWh/year}{\%\ of\ penetration}$
[0 0]	1.66788	-10.67341
[0 1.67]	1.68429	-9.16648
[0 3.35]	1.67274	-7.72745

Table C.11: Sensitivity indices of the *EUE* with respect to wind penetration for cases c_4 to c_{23}.

$\underline{\boldsymbol{\gamma}}_0^{\dagger}$	$\delta\gamma_j^w$	$\psi^u_{\gamma_j^w}\Big\vert_{\underline{\boldsymbol{\gamma}}_0} \frac{MWh/year}{\%\ of\ penetration}$
[0 5.02]	1.66220	-7.16760
[0 6.69]	1.66788	-6.43151
[0 8.35]	1.68429	-5.42007
[0 10.04]	1.67274	-4.76224
[0 11.71]	1.66222	-4.73042
[0 13.37]	3.35575	-3.65552
[0 16.73]	3.33000	-3.56847
[1.50 0]	1.66788	-6.18389
[1.50 1.67]	1.68429	-5.32925
[1.50 3.35]	1.67274	-4.65285
[1.50 5.02]	1.66220	-4.48201
[1.50 6.69]	3.35218	-3.78590
[1.50 10.04]	3.33496	-3.29719
[1.50 13.37]	3.35575	-2.71743
[1.50 16.73]	3.33000	-2.64264
[3.01 0]	1.66788	-3.90915
[3.01 1.67]	1.68429	-3.49287
[3.01 3.35]	1.67274	-3.16965
[3.01 5.02]	1.66220	-3.12658
[3.01 6.69]	1.66788	-2.56912

Table C.12: Sensitivity indices of the *EUE* with respect to wind penetration for cases c_{24} to c_{38}.

$\underline{\gamma}_0^\dagger$	$\delta\gamma_j^w$	$\psi^u_{\gamma_j^w}\Big\vert_{\underline{\gamma}_0} \frac{MWh/year}{\%\ of\ penetration}$
[3.01 8.35]	1.68429	-2.63196
[3.01 10.04]	1.67274	-2.47976
[3.01 11.71]	1.66222	-2.48644
[3.01 13.37]	3.35575	-2.21202
[3.01 16.73]	3.33000	-1.98619
[4.52 0]	3.35217	-2.69825
[4.52 3.35]	3.33494	-2.37156
[4.52 6.69]	3.35218	-2.07089
[4.52 10.04]	3.33496	-1.87109
[4.52 16.73]	3.33000	-1.40661
[6.03 0]	3.35217	-1.96082
[6.03 3.35]	3.33494	-1.92987
[6.03 6.69]	3.35218	-1.43787
[6.03 10.04]	3.33496	-1.23870

Table C.13: Sensitivity indices of the *EUE* with respect to solar penetration for cases c_1 to c_3.

$\underline{\gamma}_0^\dagger$	$\delta\gamma_j^s$	$\psi^u_{\gamma_j^s}\Big\vert_{\underline{\gamma}_0} \frac{MWh/year}{\%\ of\ penetration}$
[0 0]	0.75199	-66.17533
[0.75 0]	0.75220	-53.10791
[1.50 0]	0.75235	-43.81184

Table C.14: Sensitivity indices of the *EUE* with respect to solar penetration for cases c_4 to c_{25}.

$\underline{\gamma}_0^\dagger$	$\delta\gamma_j^s$	$\psi^u_{\gamma_j^s}\Big\vert_{\underline{\gamma}_0} \frac{MWh/year}{\%\ of\ penetration}$
[2.26 0]	0.75759	-37.01357
[3.01 0]	0.75199	-29.43399
[3.76 0]	0.75221	-26.33447
[4.51 0]	0.75235	-262.48287
[5.27 0]	0.75759	-19.16736
[0 3.35]	0.75199	-55.34536
[0.75 3.35]	0.75220	-45.38793
[1.50 3.35]	0.75235	-37.95821
[2.25 3.35]	0.75759	-33.73606
[3.01 3.35]	1.50420	-25.65158
[4.51 3.35]	1.50994	-19.18221
[0 6.69]	0.75199	-47.75215
[0.75 6.69]	0.75220	-40.20716
[1.50 6.69]	0.75235	-34.72037
[3.01 6.69]	0.75199	-25.34749
[3.76 6.69]	0.75221	-25.34749
[4.52 6.69]	0.75235	-19.27160
[0 16.73]	1.50419	-33.90991
[1.50 16.73]	1.50994	-27.15206
[3.01 16.73]	1.50420	-20.22077
[4.52 16.73]	1.50994	-13.88730

REFERENCES

[1] NERC, "Glossary of terms used in NERC reliability standards," August 2016. [Online]. Available: http://www.nerc.com/files/glossary_of_terms.pdf

[2] G. Calabrese, "Generating reserve capacity determined by the probability method," *Transactions of the American Institute of Electrical Engineers*, vol. 66, no. 1, pp. 1439–1450, Jan 1947.

[3] J. P. Pfeifenberger, K. Spees, K. Carden, and N. Wintermantel, "Resource adequacy requirements: Reliability and economic implications," September 2013. [Online]. Available: http://www.ferc.gov/legal/staff-reports/2014/02-07-14-consultant-report.pdf

[4] J. H. Nelson and L. M. Wisland, "Achieving 50 percent renewable electricity in California," August 2015, Union of Concerned Scientists. [Online]. Available: http://www.ucsusa.org/sites/default/files/attach/2015/08/Achieving-50-Percent-Renewable-Electricity-In-California.pdf

[5] "Order adopting a clean energy standard," August 2016, State of New York Public Service Commission. [Online]. Available: http://documents.dps.ny.gov/public/MatterManagement/CaseMaster.aspx?MatterCaseNo=15-e-0302

[6] J. Endrenyi, *Reliability Modeling in Electric Power Systems*. Toronto, Canada: John Wiley & Sons, 1978.

[7] C. D'Annunzio and S. Santoso, "Noniterative method to approximate the effective load carrying capability of a wind plant," *IEEE Transactions on Energy Conversion*, vol. 23, no. 2, pp. 544–550, June 2008.

[8] N. Maisonneuve and G. Gross, "A production simulation tool for systems with integrated wind energy resources," *IEEE Transactions on Power Systems*, vol. 26, no. 4, pp. 2285–2292, Nov 2011.

[9] L. L. Garver, "Effective load carrying capability of generating units," *IEEE Transactions on Power Apparatus and Systems*, vol. PAS-85, no. 8, pp. 910–919, Aug 1966.

[10] NERC, "Methods to model and calculate capacity contributions of variable generation for resource adequacy planning," March 2011. [Online]. Available: http://www.nerc.com/files/ivgtf1-2.pdf

[11] M. Milligan and B. Parsons, "A comparison and case study of capacity credit algorithms for intermittent generators," April 1997. [Online]. Available: http://www.nrel.gov/docs/legosti/fy97/22591.pdf

[12] M. Milligan and K. Porter, "Wind capacity credit in the United States," *Power and Energy Society General Meeting - Conversion and Delivery of Electrical Energy in the 21st Century, 2008 IEEE*, pp. 1–5, July 2008.

[13] NYISO, "Solar impact on grid integration: An initial assessment," June 2016. [Online]. Available: http://www.nyiso.com/public/webdocs/markets_operations/services/planning/Documents_and_Resources/Special_Studies/Special_Studies_Documents/Solar%20Integration%20Study%20Report%20Final%20063016.pdf

[14] B. Hasche, A. Keane, and M. O'Malley, "Capacity value of wind power, calculation, and data requirements: The Irish power system case," *IEEE Transactions on Power Systems*, vol. 26, no. 1, pp. 420–430, Feb 2011.

[15] R. Duignan, C. J. Dent, A. Mills, N. Samaan, M. Milligan, A. Keane, and M. O'Malley, "Capacity value of solar power," *in Proc. of 2012 IEEE Power and Energy Society General Meeting*, pp. 1–6, July 2012.

[16] J. Kleijnen, *Statistical Techniques in Simulation - Parts 1 and 2*. New York: Marcel Dekker Inc., 1974.

[17] G. Gross, "Notes for ECE 588-Electricity Resource Planning," *Univ. of Illinois at Urbana-Champaign*, Fall 2014.

[18] Y. Degeilh, "Stochastic simulation of power systems with integrated renewable and utility-scale storage resources," Ph.D. dissertation, Univ. of Illinois at Urbana-Champaign, Urbana, March 2015. [Online]. Available: http://gross.ece.illinois.edu/files/2015/03/Yannick-Degeilh.pdf

[19] R. Billinton and W. Li, *Reliability Assessment in Electric Power Systems Using Monte Carlo Methods*. New York: Springer Science & Business Media, 1994.

[20] A. Kargarian, G. Hug, and J. Mohammadi, "A multi-time scale co-optimization method for sizing of energy storage and fast-ramping generation," *IEEE Transactions on Sustainable Energy*, vol. 7, no. 4, pp. 1351–1361, Oct 2016.

[21] "Load and capacity data 2016," April 2016, New York Independent System Operator. [Online]. Available: http://www.nyiso.com/public/webdocs/markets_operations/services/planning/Documents_and_Resources/Planning_Data_and_Reference_Docs/Data_and_Reference_Docs/2016_Load__Capacity_Data_Report.pdf